Comparison of Balmer α Line Broadening and Power Balances of Helium-Hydrogen Plasma Sources

R. L. Mills*, P. Ray, M. Nansteel, B. Dhandapani, X. Chen

BlackLight Power, Inc.

493 Old Trenton Road

Cranbury, NJ 08512

ABSTRACT

From the width of the 656.3 nm Balmer α line emitted from glow discharge, Evenson microwave, MKS/Astex microwave, and inductively coupled RF plasmas, it was found that Evenson cavity microwave helium-hydrogen plasmas showed significant broadening corresponding to an average hydrogen atom energy of 180 - 210 eV with only a fast population. Inductively coupled RF helium-hydrogen plasmas showed extraordinary broadening corresponding to an average hydrogen atom energy of $250 - 310\ eV$, but the fast population was a minor component compared to the slow of $\approx 35\ eV$. The corresponding results from the glow discharge plasmas were 33 - 38 eV and 30 - 35 eV, respectively, compared to $\approx 4\ eV$ for plasmas of pure hydrogen and xenon-hydrogen maintained in any of the sources and helium-hydrogen plasmas maintained in the MKS/Astex microwave system. Stark broadening or acceleration of charged species due to high electric fields can not explain the microwave and inductively coupled RF results since the electron density was low and no high field was present. Rather, a resonant energy transfer mechanism is proposed, and the corresponding exothermic reaction was confirmed by power balance measurements. With an input of 24.8± 1 W, the total plasma power of the Evenson microwave helium-hydrogen plasma measured by water bath calorimetry was 49.1 ± 1 W corresponding to 24.3 ± 1 W of excess power in 3 cm^3. The excess power density and energy balance were high, 8.1 W/cm^3 and over $-3\ X\ 10^4\ kJ/mole\ H_2$, respectively. With an input of 500 W, a total power of 623 W was generated in a 45 cm^3 compound-hollow-cathode-glow discharge. Less than 10% excess power was observed from inductively coupled RF helium-hydrogen plasmas. No measurable heat was observed from MKS/Astex microwave helium-hydrogen plasmas.

Key Words: RF plasma, microwave plasma, glow discharge plasma, significant line broadening, power balance, resonant energy transfer mechanism

* To whom correspondence should be addressed. Phone: 609-490-1090; Fax: 609-490-1066; E-mail: rmills@blacklightpower.com

I. INTRODUCTION

Glow discharge devices have been developed over decades as light sources, ionization sources for mass spectroscopy, excitation sources for optical spectroscopy, and sources of ions for surface etching and chemistry [1-3]. A Grimm-type glow discharge is a well established excitation source for the analysis of conducting solid samples by optical emission spectroscopy [4-6]. But, only in the last decade has extensive spectroscopic characterization been conducted that has led to some puzzling observations. For example, M. Kuraica and N. Konjevic [7], Videnovic et al. [8] and others [9-12] have characterized mixed hydrogen-argon plasmas by determining the excited hydrogen atom energies and concentrations from measurements of the line broadening of the 656.3 *nm* Balmer α line. They found that the H_α lines were extremely broadened and explained the phenomenon primarily in terms of Doppler broadening due to the acceleration of charges such as H^+, H_2^+, and H_3^+ in the high fields (e. g. over $10\,kV/cm$) present in the cathode fall region.

Djurovic and Roberts [10] recorded the spectral and spatial profiles of Balmer α line emission from low pressure RF (13.56 MHz) discharges in $H_2 + Ar$ mixtures in a direction normal to the electric field. The introduction of Ar in a pure H_2 plasma increased the number of fast neutral atoms as evidenced by the intensity of the broad component of a two-component Doppler-broadened Balmer α line profile. Independent of cell position or direction, the average energy of a wide profile component was 23.8 *eV* for voltages above 100 V, and the average energy of a slow component was 0.22 *eV*. The mechanism proposed by Djurovic and Roberts is the production of fast H atoms from electric field accelerated H_2^+. The explanation of the role of Ar in the production of a large number of excited hydrogen atoms in the $n=3$ state, as well as raising their energy for a given pressure and applied RF voltage, is that collisions with Ar in the plasma sheath region enhances the production of fast H_2 from accelerated H_2^+. The fast H_2 then undergoes dissociation to form fast H which may then be excited locally to the $n=3$ state by a further collision with Ar. The local excitation is a requirement since the atomic lifetime of the hydrogen $n=3$ state is approximately $10^{-8}\,s$, and the

average velocity of the hydrogen atoms is $<10^5$ m/s. Thus, the distance traveled must be less that 0.001 m. A number of additional mechanisms have been proposed in order to explain the excessive Doppler broadening of the Balmer α line in argon-hydrogen DC or RF driven glow discharge plasmas all of which ultimately depend on electric field acceleration of hydrogen positive ions.

A new low-electric field plasma source has been developed that is based on a resonant energy transfer of an integer multiple of $27.2\,eV$ from atomic hydrogen to a catalyst capable of accepting the energy. It operates by incandescently heating a hydrogen dissociator and a catalyst to provide atomic hydrogen and gaseous catalyst, respectively, such that the catalyst reacts with the atomic hydrogen to produce a plasma called a resonant transfer (rt)-plasma. It was extraordinary, that intense EUV emission was observed [13-15] at low temperatures (e.g. $\approx 10^3\,K$) from atomic hydrogen and certain atomized elements or certain gaseous ions which singly or multiply ionize at integer multiples of the potential energy of atomic hydrogen, $27.2\,eV$ that comprise catalysts. The only pure elements that were observed to emit EUV were those wherein the ionization of t electrons from an atom to a continuum energy level is such that the sum of the ionization energies of the t electrons is approximately $m \cdot 27.2\,eV$ where t and m are each an integer. For example, K, Cs, Sr, Sr^+, and Rb^+ each ionize at integer multiples of the potential energy of atomic hydrogen and caused emission as predicted; whereas, the chemically similar atoms, Na, Mg, and Ba, do not ionize at integer multiples of the potential energy of atomic hydrogen and caused no emission as predicted as well. The theory and balanced reactions were given previously [13-17].

In addition, Ar^+ and He^+ each ionize at an integer multiple of the potential energy of atomic hydrogen; thus, a discharge with one or more of Sr^+, Ar^+, and He^+ present with hydrogen was anticipated to form an rt-plasma. Mills and Nansteel [13] have reported that rt-plasmas formed with Sr^+ and Ar^+ catalysts at 1% of the theoretical or prior known voltage requirement with a light output per unit power input up to 8600 times that of the control standard light sources. Characteristic emission was observed from Ar^{2+} and Sr^{3+} which confirmed the resonant nonradiative energy transfer of $27.2\,eV$ and $2 \cdot 27.2\,eV$ from atomic hydrogen to Ar^+ and

Sr^+, respectively [15, 18]. Predicted emission lines were observed from helium-hydrogen [16-17, 19] as well as strontium-argon-hydrogen plasmas [15, 18] that supported the rt-plasma mechanism.

He^+ ionizes at $54.417\,eV$ which is $2 \cdot 27.2\,eV$, and novel EUV emission lines were observed from microwave and glow discharges of helium with 2% hydrogen [16-17, 19]. The observed energies were $q \cdot 13.6\,eV$ ($q = 1,2,3,4,6,7,8,9,\ or\ 11$) or these energies less $21.2\,eV$ due to inelastic scattering of the lines by helium atoms in the excitation of $He\,(1s^2)$ to $He\,(1s^1 2p^1)$. These lines can be explained by the resonant transfer of 2 times $27.2\,eV$ [16-17, 19].

Line broadening and intensity of the 656.3 nm Balmer α line was measured on glow discharge, microwave, and inductively coupled RF sources to determine the excited hydrogen atom energy and H concentration in plasmas of hydrogen and a catalyst (He^+ or Ar^+) or plasmas comprising hydrogen with chemically similar controls that did not provide gaseous atoms or ions having electron ionization energies which are a multiple of $27.2\,eV$ (xenon atoms or ions). Anomalous Doppler line broadening of H_α was observed in the rt-plasmas gas mixtures and not in the controls. Moreover, as discussed *supra.*, a number of mechanisms have been proposed in order to explain the excessive Doppler broadening of the Balmer α line in argon-hydrogen high voltage DC or RF driven glow discharge plasmas that are all ultimately based on acceleration in a high electric field. We have shown previously that the experimental evidence from several rt-plasma sources does not support such a mechanism [20-21]. Many of these were shown to be untenable based on additional data and based on our previous results with microwave plasmas where no strong applied electric field (e. g. over $10\,kV/cm$) or cathode fall region is present. The observation of excessive Balmer line broadening in a microwave driven plasma requires a source of energy other than that provided by the electric field.

To further study the effect of the plasma source on the parameters of an rt-plasma for a given catalyst, 1.) the line broadening and intensity of the 656.3 nm Balmer α line was measured to determine the excited hydrogen atom energy and H concentration in plasmas of hydrogen and a He^+ catalyst compared to control xenon-hydrogen or krypton-hydrogen plasmas, and 2.) the power balance was measured.

II. EXPERIMENTAL

A. Measurement of hydrogen atom energy and number density from Balmer α line broadening and intensity of plasma sources

The width of the 656.3 nm Balmer α line was recorded on light emitted from glow discharge, Evenson cavity microwave, MKS/Astex cavity microwave, and inductively coupled RF plasmas of helium-hydrogen (90/10%) compared to pure hydrogen and xenon-hydrogen (90/10%) plasmas according to methods and setups reported previously [20-21]. Each gas was ultrahigh pure (Praxair 99.999%). The glow discharge plasmas were maintained in the cylindrical stainless steel gas cell shown in Figure 1. The 304-stainless steel cylindrical cell was 9.21 cm in diameter and 14.5 cm in height. The base of the cell contained a welded-in stainless steel thermocouple well (1 cm OD) which housed a thermocouple probe in the cell interior approximately 2 cm from the discharge and 2 cm from the cell axis. At the middle height of the cell wall was a welded-flush stainless steel tube (0.95 cm diameter) which was connected to a flexible stainless steel tube (100 cm in length) that served as a vacuum line from the cell and the line to supply the test gas. The top end of the cell was welded to a high vacuum 15.25 cm diameter conflat flange. A silver plated copper gasket was placed between a mating flange and the cell flange. The two flanges were clamped together with 10 circumferential bolts. The mating flange contained two penetrations comprising 1.) a stainless steel thermocouple well (1 cm OD) also housing a thermocouple probe in the cell interior approximately 2 cm from the discharge and 2 cm from the cell axis and 2.) a centered high voltage feedthrough which transmitted the power, supplied through a power connector, to a hollow cathode inside the cell.

The axial hollow cathode glow discharge electrode assembly comprised a stainless steel plate (42 mm diameter, 0.9 mm thick) anode and a circumferential stainless steel cylindrical frame (5.08 cm OD, 7.2 cm long) perforated with evenly spaced 1 cm diameter holes which served as the cathode. The cathode was attached to the cell body by a stainless steel wire, and the cell body was grounded.

A 1.6 mm thick UV-grade sapphire window with 1.5 cm view diameter provided a visible light path from inside the cell. The viewing direction was normal to the cell axis.

The cell was evacuated with a turbo vacuum pump to a pressure of 4 mTorr, and pressurized with the test gas to 2 Torr total pressure. The pressure of each test gas comprising a mixture with 10% hydrogen was determined by adding the pure noble gas to a given pressure and increasing the pressure with hydrogen gas to a final pressure. The partial pressure of the hydrogen gas was given by the incremental increase in total gas pressure monitored by a 0-10 Torr absolute pressure gauge. The discharge was carried out under static gas conditions. The discharge was started and maintained by a DC electric field supplied by a constant voltage DC power supply at 275 V which produced a current of about 0.2 A. In the case of helium-hydrogen plasmas, the voltage was increased at 50 V increments from 275 V to 475 V, and the high resolution visible spectra were recorded to observe the effect of voltage on the Balmer α line broadening.

Balmer α line broadening was measured at Jobin Yvon Horiba, Inc, Edison, NJ. The plasma emission from the glow discharges of pure hydrogen and noble gas-hydrogen mixtures was fiber-optically coupled through a 220F matching fiber adapter to a TRIAX 550 Spectrometer with a standard PMT detector that had a resolution of $\pm 0.025\,nm$ over the spectral range $190\text{-}860\,nm$. The entrance and exit slits were set to $20\,\mu m$. The spectrometer was scanned between $656\text{-}657\,nm$ using a $0.01\,nm$ step size. The signal was recorded by a PMT (Hamamatsu R928) with a stand alone high voltage power supply (950 V) and an acquisition controller (SpectrAcq 2). The data was obtained in a single accumulation with a 1 second integration time.

The Evenson microwave plasmas were maintained in the microwave discharge cell light source shown in Figure 2. Each test gas or mixture was flowed through a half inch diameter quartz tube at 300 mTorr maintained with a noble gas flow rate of 9.3 sccm or a noble gas flow rate of 8.3 sccm and a hydrogen flow rate of 1 sccm. Each gas flow was controlled by a 0-20 sccm range mass flow controller (MKS 1179A21CS1BB) with a readout (MKS type 246). The cell pressure was monitored by a 0-10 Torr MKS Baratron absolute pressure gauge. The

tube was fitted with an Opthos coaxial microwave cavity (Evenson cavity). The microwave generator shown in Figure 2 was an Opthos model MPG-4M generator (Frequency: 2450 MHz). The input power to the plasma was set at 40 watts with forced air cooling of the cell. In separate experiments, the power was increased up to 100 W to determine the relationship between input power and Balmer α line broadening.

The Balmer α line widths were recorded on light emitted from helium-hydrogen (98/2%) compared to pure hydrogen plasmas maintained in an MKS/Astex AX7610 microwave plasma applicator shown in Figure 3. Microwave power was delivered to the plasma applicator through a waveguide system comprising a 1.5 kW MKS/Astex microwave power generator and magnetron (AX2115), circulator (AX3120), and stub tuner (AX3041). The broadening experiments were repeated using a 5 kW system replacing the 1.5 kW system wherein the power was supplied by an MKS/Astex AX2040 generator and magnetron with an AX3021 circulator and WR340 waveguide. Reflected power returning to the circulator was sensed by a -50 dB directional coupler mounted on the circulator upstream of a dummy load. Nominal forward and reflected power magnitudes were indicated on the generator front panel. The system was operated at 1000 W net input power (forward minus reflected power) with less that 3% reflected power. The flow of test gas through the applicator was controlled by MKS 10 and 100 sccm mass flow controllers. The controllers were special-calibrated for hydrogen and helium with a bubble flow meter. Uncertainty in gas flow rate was no greater than ±2%. Gas stream pressure was monitored with a 10 Torr MKS Baratron absolute pressure gauge just downstream of the applicator as shown in Figure 3. The gas flow rate was 50 sccm for He/H_2 and 10 sccm for pure H_2. The pressure was either 0.5 or 1 Torr. Process gas was exhausted from the applicator through a Drivac turbine vacuum pump. This allowed for evacuation of the system to a pressure level of approximately 5 mTorr under no-flow conditions. Gas pressure in the applicator was controlled by throttling through an MDC KAV-100 angle valve on the vacuum pump inlet. Spectroscopic measurements were made radially through optical access ports in the applicator body located 9 cm upstream and downstream of the waveguide, and also axially

through a 25 mm diameter sapphire viewport at one end of the applicator as shown in Figure 4.

The width of the 656.3 nm Balmer α line emitted from inductively coupled RF discharges of helium-hydrogen (90/10%) was compared to pure hydrogen and xenon-hydrogen (90/10%) plasmas maintained in an inductively coupled RF discharge gas cell light source shown in Figure 5. A quartz cell which was 500 mm in length and 50 mm in diameter served as the plasma reactor. A Pyrex cap sealed to the quartz cell with a Viton O ring and a C-clamp incorporated ports for gas inlet, outlet, and photon detection. An unterminated, nine-turn, 17 cm long helical coil (18 gauge magnet wire) wrapped around the outside of the cell was connected to a 13.56 MHz RF generator (RF VII, Inc., Model MN 500) with a matching network (RF Power Products, Inc., Model RF 5S, 300 W). The coil inductance and resistance were $4.7\,\mu H$ and $0.106\,\Omega$, respectively. The coil impedance was $400\,\Omega$ at 13.56 MHz. The input power was 60 W, and the reflected power was less than 1 W. In separate experiments, the power was varied from 40 to 100 W to determine the relationship between input power and Balmer α line broadening. The gas flow rate and pressure were 5.5 sccm and 300 mTorr, respectively, using the flow meters and pressure gauges of the Evenson cell.

The plasma emission from the Evenson cavity microwave, MKS/Astex system microwave, and inductively coupled RF plasmas was fiber-optically coupled through a 220F matching fiber adapter positioned 2 cm from the cell wall to a visible spectrometer with a resolution of $\pm 0.006\,nm$ over the spectral range $190\text{-}860\,nm$. The spectrometer was a Jobin Yvon Horiba 1250 M with 2400 groves/mm ion-etched holographic diffraction grating. The entrance and exit slits were set to $20\,\mu m$. To measure the Balmer α line width, the spectrometer was scanned between 655.5 and 657 nm using a $0.005\,nm$ step size. The signal was recorded by a PMT with a stand alone high voltage power supply (950 V) and an acquisition controller. The data was obtained in a single accumulation with a 1 second integration time. The line width was also recorded on the Balmer β, γ, and δ lines at 486.14, 434.05, and 410.18 *nm*, respectively, and *He* I lines at 706.517, 667.816, 587.56, 447.15, and 402.62 *nm*.

To measure the absolute intensity, the high resolution visible

spectrometer and detection system were calibrated [22] with 546.08 *nm*, 576.96 *nm*, and 696.54 *nm* light from a Hg-Ar lamp (Ocean Optics, model HG-1) that was calibrated with a NIST certified silicon photodiode. The population density of the $n=3$ hydrogen excited state N_3 was determined from the absolute intensity of the Balmer α (656.28 *nm*) line measured using the calibrated spectrometer. The spectrometer response was determined to be approximately flat in the 4000-7000 Å region by ion etching and with a tungsten high intensity calibrated lamp.

The method of Videnovic et al. [8] and also originally after Griem [23] was used to calculate the energetic hydrogen atom energies from the width of the 656.3 *nm* Balmer α line emitted from glow discharge, microwave, and inductively and capacitively coupled RF discharge plasmas. The full half-width $\Delta\lambda_G$ of each Gaussian results from the Doppler ($\Delta\lambda_D$) and instrumental ($\Delta\lambda_I$) half-widths:

$$\Delta\lambda_G = \sqrt{\Delta\lambda_D^2 + \Delta\lambda_I^2} \tag{1}$$

$\Delta\lambda_I$ in our experiments was $\pm 0.025\,nm$ in the case of the glow discharge cells and $\pm 0.006\,nm$ otherwise. The temperature was calculated from the Doppler half-width using the formula:

$$\Delta\lambda_D = 7.16\,X\,10^{-7}\lambda_0\left(\frac{T}{\mu}\right)^{1/2} \quad (nm) \tag{2}$$

where λ_0 is the line wavelength in nm, T is the temperature in K ($1\,eV = 11{,}605\,K$), and μ is the atomic weight (=1 for hydrogen). In each case, the average Doppler half-width that was not appreciably changed with pressure varied by ±5% corresponding to an error in the energy of ±10%.

The H number density for $n=1$ was estimated using the absolute density of $n=3$ by the following equation which is in good agreement with the evolution equations of Sultan et al. [24]:

$$\frac{[H(n=3)]}{[H(n=1)]} = \frac{g_3}{g_1}\exp(-\Delta E/kT) \tag{3}$$

where the degeneracy g is given by $g=2n^2$ (n is the principal quantum number) and $kT \approx 1\,eV$. The number densities varied by ±20% depending on the pressure.

The electron density and temperature of the rt-plasma was determined using a compensated Langmuir probe according to the method given previously [25].

B. Power balances of plasma sources

Power balances were recorded on glow discharge, Evenson cavity microwave, MKS/Astex system microwave, and inductively coupled RF plasmas of helium-hydrogen compared to control plasmas of krypton, krypton-hydrogen, xenon, or xenon-hydrogen. Power balances of helium-hydrogen (95/5%) glow and krypton-hydrogen (95/5%) discharge plasmas were compared to an ohmic heater control. The plasmas were maintained in the cylindrical stainless steel gas cell shown in Figure 6 operated under flow conditions, and the power was measured by heat loss calorimetry as the input power was varied. The experimental setup for generating a glow discharge plasma and for measuring the power balance is shown in Figure 7. All experiments were performed in a kiln shown in Figure 7 maintained at a controlled constant temperature of 200.0°C.

The 304-stainless steel cylindrical cell was 9.21 cm in diameter and 14.5 cm in height. The base of the cell contained a welded-in stainless steel thermocouple well (1 cm OD) which housed a thermocouple probe in the cell interior approximately 2 cm from the discharge and 2 cm from the cell axis. Also, a reentrant stainless steel tube (0.64 cm diameter) was at the base of the cell wall and was connected to a flexible stainless steel tube (100 cm in length) that served as a vacuum line from the cell. The top end of the cell was welded to a high vacuum 15.24 cm diameter conflat flange. A silver plated copper gasket was placed between a mating flange and the cell flange. The two flanges were clamped together with 10 circumferential bolts. The mating flange contained three penetrations comprising 1.) a stainless steel thermocouple well (1 cm OD) also housing a thermocouple probe in the cell interior approximately 2 cm from the discharge and 2 cm from the cell axis, 2.) a centered high voltage feedthrough which transmitted the power, supplied through a power connector, to a compound hollow cathode inside the cell, and 3.) a stainless steel reentrant tube (0.64 cm diameter and 100 cm in length) welded flush with the bottom surface of the top flange that served as the line to supply the test gas.

The diameter of the inlet and vacuum outlet were selected to be

0.64 cm which allowed for adequate flow while minimizing the formation of plasma in these tubes. In addition, the inlet and outlet tubes comprised reentrant tubes which extended significantly into the cell such that any plasma which formed in these tubes was contained within the cell. Thus, any heat which evolved due to plasma formation in these tubes was also contained in the cell.

The axial compound hollow cathode glow discharge electrode assembly shown in Figure 6 comprised a bundle of 19 tubes packed concentrically within a larger support tube and located adjacent to a planar anode disk. The bundled tubes were 316 stainless steel with outer diameter 0.953 cm, 0.89 mm wall thickness, and 5.1 cm length. A close-packed arrangement was used in which each interior tube in the bundle was surrounded by and was in contact with six neighboring tubes. The bundle was rigidly constructed by spot welding contacting tube pairs at the bundle ends. The 46 mm diameter tube bundle was fixed concentrically within the 48 mm ID stainless steel support tube by three set screws which passed radially through the support tube wall, making electrical contact with the bundle and support tube. The assembly was completed by a 316 stainless steel anode disk located concentrically within the support tube and oriented normal to the axis of the support tube/tube bundle assembly. The 42 mm diameter, 0.91 mm thick anode disk was electrically isolated from the support tube by a uniform annular gap of approximately 3 mm between the outer edge of the anode disk and the inner surface of the support tube. The anode disk and tube bundle end plane were separated by a distance of approximately 1 cm. The compound hollow cathode assembly consisting of the support tube, tube bundle, and anode disk was located on the axis of the cell. The tube bundle, support tube and cell body were maintained at ground potential while voltage for the anode disk was supplied by the high voltage feed-through on the cell upper flange. A spectroscopic viewport described previously for similar cells [13, 20] was not present in these experiments.

The cell was evacuated with a turbo vacuum pump to a pressure of <1 mTorr. The gas pressure inside the cell was maintained at 1 Torr with test gas flow rate of 2 sccm. Ultra-high pure, premixed helium-hydrogen (95/5%) was used for both the plasma and heater control experiments. Ultra-high pure, premixed krypton-hydrogen (95/5%) was used as a

control gas. The gas flow was controlled by a mass flow controller. The cell pressure was monitored by an absolute pressure gauge.

The discharge was started and maintained by a DC electric field in the compound hollow cathode supplied by a constant voltage DC power supply (Xantrex XRF 600-2). The input power was calculated as the product of the constant voltage times the current. The voltage between the cathode and anode was monitored by a digital multimeter (Digital Instruments 9300GB). A duplicate multimeter in series with the discharge gap was used to indicate the current. The power was increased by ramping the constant voltage.

The ohmic calibration heater comprised a 225 cm long, 0.25 mm diameter tungsten filament that was coiled on a 33 mm OD alumina support tube mounted inside the bundle support tube. The heater was powered by a Xantrex DC power supply over the power range 10-400 ± 0.1 W.

The temperature response of the cell to input power for the test and control gas mixtures and the ohmic heater control was determined. The temperature at the two thermocouples was recorded and averaged about one hour after the cell had reached a thermal steady state. The time to reach a steady state temperature with each increase in the input power to the glow discharge was typically 3-4 hours. At this point, the power P_{out} lost from the cell was equal to the power supplied to the cell P_{in} plus any excess power P_{ex}.

$$P_{out} = P_{in} + P_{ex} \tag{4}$$

The rate of heat loss from the cell was of the form

$$P_{out} = a(T - T_0) + b(T^4 - T_0^4) \tag{5}$$

where T was the cell temperature, $T_0 = 200.0\ °C = 473.2\ K$ was the fixed kiln temperature, and a and b are parameters. The first term on the right corresponds to heat loss by conduction and convection, and the second term corresponds to radiation heat loss. Expanding and rearranging results in

$$P_{out} = (a + 4bT_0^3)\Delta T + b\left[6(T_0\Delta T)^2 + 4T_0\Delta T^3 + \Delta T^4\right] \tag{6}$$

where $\Delta T = T - T_0$ is the cell temperature rise above the kiln temperature. The rate of heat loss from the cell in the case of the ohmic heater was identical to the measured electrical power input ($P_{ex} = 0$).

ΔT was recorded as a function of input power P_{in} for the ohmic heater control over the input power range of 100 to 400 W. The higher temperature produced by the helium-hydrogen plasmas compared with the heater calibration and the krypton-hydrogen plasma control was representative of the excess power since the cell temperature rise was found to be insensitive to heat transfer mechanisms occurring inside of the cell—the transfer to the cell walls being very fast and heat loss from the wall to the outside ambient environment dominating the cell temperature. In the case of each catalyst run, the total output power P_{out} was determined by solving Eq. (6) using the measured ΔT. The excess power P_{ex} was determined from Eq. (4).

For the Evenson-cavity microwave plasma, the excess power was measured by water bath calorimetry on helium-hydrogen (90/10%) plasmas compared to krypton plasma with the same input power. The plasmas were maintained in a microwave discharge cell shown in Figure 8. Each gas was ultrahigh pure. Each pure test gas was flowed through a half inch diameter quartz tube at 500 mTorr maintained with a noble gas or hydrogen flow rate of 10 sccm. After the calorimeter had reached a steady state, the pressure of the helium-hydrogen mixture was changed to 0.29 Torr. Each gas flow was controlled by a 0-20 sccm range mass flow controller (MKS 1179A21CS1BB) with a readout (MKS type 246). The cell pressure was monitored by a 0-10 Torr MKS Baratron absolute pressure gauge. The tube was fitted with an Evenson coaxial microwave cavity (Opthos) having an E-mode [26-27]. The microwave generator shown in Figure 8 was an Opthos model MPG-4M generator (Frequency: 2450 MHz).

The Evenson cavity and a plasma-containing section of the quartz tube were fitted with a water-tight stainless steel housing shown in Figure 8. The housing comprised a 4X4X2 cm rectangular enclosure welded to a set of high vacuum 15.24 cm diameter conflat flanges. A silver plated copper gasket was placed between a mating flange and the cell flange. The two flanges were clamped together with 10 circumferential bolts. The top mating flange contained two penetrations comprising 1.) a stainless steel thermocouple well (1 cm OD) housing a thermocouple probe in the cell interior that was in contact with the quartz tube wall adjacent to the Evenson cavity and 2.) a centered 2.54

cm OD coaxial cable housing. The 1.27 cm OD quartz tube was sealed at its penetrations with the rectangular housing by Ultratorr fittings. The housing and cell assembly was suspended by 4 support rods from an 5.1 cm thick acrylic plate which held the cell vertically from the top of a water bath calorimeter shown in Figure 8. The plate contained four sealed penetrations comprising 1.) the stainless steel thermocouple well 2.) a 1 cm OD noble or hydrogen gas line, 3.) a 1 cm OD vacuum line, and 4.) the 2.54 cm OD coaxial cable housing. The gas inlet connected to a 0.64 cm OD flexible stainless steel tube that was connected by an Ultratorr seal to a welded-in 0.63 cm OD penetration of the rectangular enclosure. Inside of the enclosure, the penetration connected to the quartz tube by a 0.63-to-1.27 cm OD mating Ultratorr seal. The quartz tube had an elbow at the end opposite to the gas inlet penetration which attached to a 1 cm OD flexible stainless steel tube section of the vacuum line. The microwave cavity contained in the rectangular enclosure was tuned by a threaded tuning stub sealed in an end wall of the enclosure and a sliding tuning stub sealed with an Ultratorr fitting in the bottom wall. The sliding stub was tightened after the cell was tuned outside of the water bath, and the cell was immersed.

The water bath comprised an insulated reservoir filled with 45 liters of distilled water. The water was agitated with a paddle driven by a stirring motor. A high precision linear response thermistor probe (Omega OL-703) recorded the temperature of the water bath as a function of time for the stirrer alone to establish the baseline. The water bath was calibrated by a high precision heater (Watlow 125CA65A2X, with a Xantrex DC power supply 0-1200 ± 0.01 W). The heat capacity was determined for several input powers, 30, 40, and 50 W ± 0.01 W, and was found to be independent of input power over this power range within ± 0.05%. The temperature rise of the reservoir as a function of time gave a slope in °C/s. This slope was baseline corrected for the negligible stirrer power and loss to ambient. The constant known input power (J/s), was divided by this slope to give the heat capacity in J/°C. Then, in general, the total power output from the cell to the reservoir was determined by multiplying the heat capacity by the rate of temperature rise (°C/s) to give J/s.

Since the cell and water bath system were adiabatic, the general

form of the power balance equation is given by Eq. (4) where P_{in} is the microwave input power, P_{ex} is the excess power generated from the hydrogen catalysis reaction, and P_{out} is the thermal power loss from the cell to the water bath. The cell typically reached steady state in about 10 minutes after each experiment was started. At this point, the power lost from the cell P_{out} was equal to the power supplied to the cell, P_{in}, plus any excess power P_{ex} as given by Eq. (4). Since the cell was surrounded by water that was contained in an insulated reservoir with negligible thermal losses, the temperature response of the thermistor T as a function of time t was modeled by a linear curve

$$\dot{T}(t) = c^{-1} P_{out} \tag{7}$$

where c is the heat capacity (J/°C) for the least square curve fit of the response to power input for the control experiments ($P_{ex} = 0$). The slope was recorded for about 2 hours after the cell had reached a thermal steady state, to achieve an accuracy of ± 1%.

The slope of the temperature rise as a function of time was recorded for each run and baseline corrected for the negligible stirrer power and loss to ambient, then the output power was calculated from the corrected slope. After the calorimeter was calibrated, $T(t)$ was recorded with a selected setting of the forward and reflected power to the krypton plasma. The slope was determined with this constant forward and reflected microwave power, and the microwave input power was absolutely determined for these panel meter readings using Eq. (7) with the $\dot{T}(t)$ response and the heat capacity c. Then, identical forward and reflected microwave power settings were replicated for the helium-hydrogen mixture and $T(t)$ was again recorded. The higher slope produced with helium-hydrogen mixture, having He^+ as a catalyst and atomic hydrogen as a reactant, compared with controls with no hydrogen and no catalyst present was representative of the excess power. In the case of the catalysis run, the total output power P_{out} was determined by solving Eq. (7) using the measured $\dot{T}(t)$ and the heat capacity c. The excess power P_{ex} was determined from Eq. (4).

Power balances were measured on plasmas of helium and xenon and 2 to 10% hydrogen mixed with helium and xenon maintained in the MKS/Astex AX7610 microwave plasma applicator with the 1.5 kW system. The applicator comprised a 25 mm quartz tube housed

concentrically within a cylindrical cavity and oriented normal to the axis of a rectangular waveguide. The outer surface of the quartz tube was wrapped with copper tubing of square cross section as shown in Figure 4. The spiral copper tubing was bonded to the exterior surface of the quartz tube by a thin layer of RTV that permitted excellent thermal coupling between the plasma and the coolant stream. The applicator body was insulated with 25 mm thick elastomer foam to minimize heat loss to the surroundings. Thermal power rejection from the plasma in the applicator was measured by water flow calorimetry. A constant water flow rate from a supply to the applicator was maintained using a water pressure regulator shown in Figure 3. The water flow rate through the system was monitored by a Gilmont variable area flow meter with ±2% accuracy and ±1% repeatability. The water stream temperature rise in the applicator was monitored by precision calibrated type 44032 thermistor probes located at the applicator water inlet and exit that were accurate to ±0.1°C. Probe resistance was measured by a voltage divider circuit incorporating 20 and 100 kOhm precision (0.1%) resistors. Uncertainty in the measurement of water stream temperature rise was less than ±1% and uncertainty in the measurement of thermal power absorption by the water was less than ±3%. Gas stream inlet and exit temperature were also monitored with thermistor probes. Both gas and water inlet and exit temperatures were continuously recorded by a DAS.

After initiating gas flow, several minutes were allowed for pressure and flow rate to stabilize. Water flow to the applicator was set at 0.66 liter/min before activating the microwave power. Microwave power levels of ~200 W or more resulted in spontaneous gas breakdown and plasma formation in the quartz tube of the applicator. The presence of plasma was verified by visual inspection and also by a sharp decrease in indicated reflected power which accompanied breakdown. After setting the desired forward power, adjustment of the 3-stub tuner was made in order to minimize the reflected power. It was always possible to reduce reflected power to less than 3%, and usually less than 1%, of forward power in this way. Variations in net power delivery to the applicator during the course of a run were typically less than 1%. Thermal response of the applicator and coolant stream was quite rapid. The presence of thermal steady state was determined by monitoring the water exit

temperature from the applicator as a function of time and was usually achieved in less than 30 min.

The power balance of helium-hydrogen (95/5%) RF plasmas compared to xenon was measured by water bath calorimetry. The calorimetry methods were the same as those used to record the power balance on the microwave cell, but the microwave cell and housing were replaced by the inductively coupled RF cell shown in Figure 5 that was placed in a water-tight bag that comprised an aluminum layer between two plastic lamina.

III. Results

A. Hydrogen atom energy and number density from Balmer α line broadening and intensity of plasma sources

a. Balmer α line broadening recorded on glow discharge plasmas

The 656.3 nm Balmer α line width was measured for glow discharge light sources with a high resolution ($\pm 0.025\ nm$) visible spectrometer. The discharge was started and maintained at 2 Torr total pressure by a DC electric field supplied by a constant voltage DC power supply at 275 V which produced a current of about 0.2 A. The 656.3 nm Balmer α line width recorded on glow discharge plasmas of hydrogen compared with each of xenon-hydrogen (90/10%) and helium-hydrogen (90/10%) are shown in Figures 9 and 10, respectively. The energetic hydrogen atom energies and hydrogen atom densities of the plasmas of hydrogen alone and hydrogen-noble gas mixtures are given in Table 1. It was found that helium-hydrogen showed significant broadening corresponding to an average hydrogen atom energy of $30\text{-}38\ eV$ and an atom density of $3 X 10^{13} \pm 20\%\ atoms/cm^3$; whereas, pure hydrogen and xenon-hydrogen showed no excessive broadening corresponding to an average hydrogen atom energy of $\approx 4\ eV$. The maximum atom density of only $5 X 10^{13} \pm 20\%\ atoms/cm^3$ was observed with pure hydrogen as the test gas even though 10 times more hydrogen was present. No voltage or power effect on the broadening was observed with the helium-hydrogen

plasmas over the range studied.

b. Balmer α line broadening measurements recorded on Evenson microwave discharge plasmas

The 656.3 nm Balmer α line width recorded with a high resolution ($\pm 0.006\ nm$) visible spectrometer on microwave discharge plasmas of hydrogen compared with each of xenon-hydrogen (90/10%) and helium-hydrogen (90/10%) are shown in Figures 11 and 12, respectively. The statistical curve fit of each of the hydrogen plasma and the helium-hydrogen plasma emission matched a Gaussian profile. The energetic hydrogen atom energies and H densities of plasmas of hydrogen alone and noble gas-hydrogen mixtures are given in Table 1. It was found that the helium-hydrogen microwave plasmas showed extraordinary broadening corresponding to an average hydrogen atom energy of $180\text{-}210\ eV$ and an atom density of $4.8\ X\ 10^{14} \pm 20\%\ atoms/cm^3$. Whereas, pure hydrogen and xenon-hydrogen showed no excessive broadening corresponding to an average hydrogen atom energy of $\approx 4\ eV$. The maximum atom density of only $7\ X\ 10^{13} \pm 20\%\ atoms/cm^3$ was observed with pure hydrogen as the test gas which was less than that of the helium-hydrogen and argon-hydrogen plasmas even though 10 times more hydrogen was present in the pure hydrogen plasma. The broadening was not found to depend on the input power over the range studied. Furthermore, only the hydrogen lines were broadened. The addition of hydrogen to helium had no effect on the helium lines as shown for the 667.816 *nm He* I line in Figure 13.

Excessive line broadening was only observed in the cases where an ion was present which could provide a net enthalpy of reaction of an integer multiple of the potential energy of atomic hydrogen (He^+). Whereas, excess line broadening was not observed for plasmas of chemically similar controls that do not provide gaseous atoms or ions that have electron ionization energies which are a multiple of $27.2\ eV$ (atoms or ions of *Xe*). The broadening observed for the first time in $He-H_2$ plasmas was predicted. The absence of broadening in the control plasmas was predicted as well. Thus, these results support the rt-plasma mechanism.

We have assumed that Doppler broadening due to thermal motion was the dominant source to the extent that other sources may be neglected. This assumption was confirmed when each source was considered. In general, the experimental profile is a convolution of two Doppler profiles, an instrumental profile, the natural (lifetime) profile, Stark profiles, van der Waals profiles, a resonance profile, and fine structure. The contribution from each source was determined to be below the limit of detection [20-21].

Furthermore, no hydrogen species, H^+, H_2^+, H_3^+, H^-, H, or H_2, responds to the microwave field; rather, only the electrons respond. But, the Langmuir probe measured electron temperature was about 1 eV; whereas, the measured H temperature was $180\text{-}210\,eV$. This requires that $T_H >>> T_e$. This result can not be explained by electron or external Stark broadening or electric field acceleration of charged species. The electron density was five orders of magnitude too low [20-21]. And, in microwave driven plasmas, there is no high electric field in a cathode fall region ($>1\,kV/cm$) to accelerate positive ions as proposed previously [7-12] to explain significant broadening in hydrogen containing plasmas driven at a high voltage electrode. It is impossible for H or any H-containing ion which may give rise to H to have a higher temperature than the electrons in a microwave plasma. The observation of excessive Balmer line broadening in a microwave driven plasma requires a source of energy other than that provided by the electric field. We propose that the source is the hydrogen catalysis reaction followed by subsequent reactions to further lower energy states given previously [16-17, 19].

The formation of fast H can be explained by a resonant energy transfer from hydrogen atoms to He^+ ions of two times the potential energy of atomic hydrogen, $2 \cdot 27.2\,eV$, followed by a collisional energy transfer to yield fast $H(n=1)$ as well as the emission of $q \cdot 13.6\,eV$ photons discussed previously [16-17, 19]. For example, the exothermic chemical reaction of $H+H$ to form H_2 does not occur with the emission of a photon. Rather, the reaction requires a collision with a third body, M, to remove the bond energy-$H+H+M \rightarrow H_2+M^*$ [28]. The third body distributes the energy from the exothermic reaction, and the end result is the H_2 molecule and an increase in the temperature of the system. In the case of the catalytic hydrogen reaction with the formation of states given

previously [16-17, 19], the temperature of H becomes very high.

The hydrogen atom energy in plasmas of hydrogen mixed with helium were about 50-100 times that observed for the control plasmas such as hydrogen mixed with xenon or hydrogen alone. Even so, the observed $\approx 4\,eV$ energy of the latter plasmas was still well above the resolution capability of the instrument, and surprisingly it was appreciably above that expected based on the electron temperature of 1-2 eV. The observation of an elevated hydrogen atom energy for pure hydrogen plasmas and mixtures containing hydrogen with the unusual absence of an elevated energy of any other gas present has been observed before [20-21]. Since the ionization energy of hydrogen is $13.6\,eV$, two hydrogen atoms can provide a net enthalpy equal to the potential energy of the hydrogen atom, 27.2 eV—the necessary resonance energy, for a third hydrogen atom. On this basis, the unusual observation of the H energy slightly above the electron temperature is expected as discussed previously [20-21].

c. Balmer α line broadening measurements recorded on MKS/Astex microwave discharge plasmas

The 656.3 nm Balmer α line width was recorded with a high resolution ($\pm 0.006\,nm$) visible spectrometer on microwave discharge plasmas of hydrogen compared with helium-hydrogen (98/2%) maintained with the 1.5 kW and 5 kW MKS/Astex systems. Axial and radial spectra were obtained using both systems, and the spectra were independent of the system at the same input power, but the mode of observation showed different results. The 656.3 nm Balmer α line width recorded radially on 1.5 kW-system MKS/Astex microwave discharge plasmas of hydrogen compared with helium-hydrogen (98/2%) with 150-1000 W input power at 0.5 and 1 Torr are shown in Figure 14. The line broadening of the helium-hydrogen plasma was completely negligible at 0.5 Torr and 150 W. At 1000 W microwave input, the Balmer line width (FWHM) for helium-hydrogen (98/2%) was broadened by about 0.3 and 0.1 Å compared with pure hydrogen for plasmas at 1 and 0.5 Torr, respectively.

The 656.3 nm Balmer α line width recorded axially on 5 kW-

system MKS/Astex microwave discharge plasmas of hydrogen compared with helium-hydrogen (98/2%) at 1000 W input power and 0.5 and 1 Torr are shown in Figure 15. At 1000 W, the Balmer line width of the helium-hydrogen plasma was broadened by 0.5 and 0.9 Å at 1 and 0.5 Torr, respectively. The line broadening of the axial spectra was greater than that of the radial spectra since emission from the entire plasma column was incident on the detector, including the central applicator zone adjacent to the waveguide where microwave power deposition may be more intense.

d. Balmer α line broadening measurements recorded on inductively coupled RF discharge plasmas

The 656.3 nm Balmer α line width recorded with a high resolution ($\pm 0.006\ nm$) visible spectrometer on inductively coupled RF discharge plasmas of hydrogen compared with xenon-hydrogen (98/10%) and helium-hydrogen (98/10%) are shown in Figures 16 and 17, respectively. The energetic hydrogen atom energies and H densities of plasmas of hydrogen alone and noble gas-hydrogen mixtures are given in Table 1. It was found that the inductively coupled RF helium-hydrogen plasmas showed a much greater intensity and extraordinary broadening corresponding to an average fast hydrogen atom energy of $250-310\ eV$ and an atom density of $7.5\ X\ 10^{14} \pm 20\%\ atoms/cm^3$. Whereas, pure hydrogen and xenon-hydrogen showed no excessive broadening corresponding to an average hydrogen atom energy of $\approx 4\ eV$. The maximum atom density of only $9\ X\ 10^{13} \pm 20\%\ atoms/cm^3$ was observed with pure hydrogen as the test gas even though 10 times more hydrogen was present.

The hydrogen plasma emission was statistically well fit by a single Gaussian curve; whereas, the helium-hydrogen plasma emission matched two Gaussian profiles. Significant broadening was observed for both curves corresponding to slow and fast hydrogen atoms having an average hydrogen atom energy of $35-40\ eV$ and $250-310\ eV$, respectively, as shown in Table 1. However, the broadened populations were found to be in a relatively small volume corresponding to the maximum brightness of the plasma and were found to be very dependent on plasma conditions such as pressure and hydrogen concentration.

These studies demonstrate excessive line broadening in the absence of an observable effect attributable to a strong electric field since the hydrogen emission shows no broadening. No power or voltage dependence of the broadening was observed over the range studied, 40-100 W and RF voltages of about 40 V [21].

B. Power balances of plasma sources

a. Glow discharge cell power balance measurements

The plot of the discharge cell temperature increase above the constant kiln temperature of 200.0 °C as a function of the power applied to the gas mixtures and the ohmic calibration heater at 1 Torr total pressure is shown in Figure 18. Fitting the parameters a and b of Eq. (6) to the ΔT and P_{in} data for the heater given in Table 2 yielded

$$P_{out} = (1.277\ W/K)\Delta T + (2.112\ X\ 10^{-9}\ W/K^4)\left[6(T_0\Delta T)^2 + 4T_0\Delta T^3 + \Delta T^4\right] \quad (8)$$

with an rms deviation of the data from the curve fit of 0.9 W as shown in Figure 18. Compared to the heater calibration, no excess heat was observed for krypton-hydrogen glow discharge plasmas. In contrast, excess power was observed for helium-hydrogen plasmas. The power generated by the helium-hydrogen (95/5%) plasma corresponding to a cell temperature rise ΔT is the difference between the rate of heat loss from the cell and the measured power input $P_{He/H_2}(\Delta T)$:

$$P_{ex}(\Delta T) = P_{out}(\Delta T) - P_{He/H_2}(\Delta T) \quad (9)$$

Power generation for the helium-hydrogen plasma is given in Table 3. For a power input to the glow discharge of 500 W, the excess output power was $123 \pm 5\ W$ based on a comparison of the temperature rise of the cell with helium-hydrogen (95/5%) mixture and calibration heater. As shown in Figure 18 and Table 3, the excess power increased disproportionately with increasing input power. Since the hydrogen flow rate was 0.1 sccm, an estimate of the corresponding energy balance at $123 \pm 5\ W$ excess power was over $-1\ X\ 10^6\ kJ/mole\ H_2$ compared to the enthalpy of combustion of hydrogen of $-241.8\ kJ/mole\ H_2$. The results were found to be repeatable in separate experiments.

b. Evenson microwave cell power balance measurements

The thermogram, $T(t)$ response of the cell, with stirring only and with a constant input power to the high precision heater of 50 W is shown in Figure 19. The baseline corrected least squares fit of the slope, $\dot{T}(t)$, was $2.622\,X\,10^{-4}\ °C/s$, and the heat capacity determined from Eqs. (4) and (7) with $P_{ex}=0$, and $P_{in}=P_{out}=50\,W$ was $1.907\,X\,10^{5}\,J/°C$. Then the temperature response of the calorimeter for any case (Eq. (7)) was determined to be

$$\dot{T}(t)=\left(1.907\,X\,10^{5}\,J/°C\right)^{-1}\times P_{out} \qquad (10)$$

The $T(t)$ water bath response to stirring and then with selected panel meter readings of the constant forward and reflected microwave input power to krypton was recorded as shown in Figure 20. Using the corresponding $\dot{T}(t)$ in Eq. (10), the microwave input power was determined to be 24.8± 1 W. A helium-hydrogen (90/10%) mixture was run at the same microwave input power readings as the control which corresponded to $P_{in}=24.8\pm1\,W$ in Eq. (4). The $T(t)$ response was significantly increased for helium-hydrogen (90/10%) as shown in Figure 20. The output power was determined to be 49.1 ± 1 W from the corresponding $\dot{T}(t)$ using Eq. (10). From Eq. (4), the excess power was 24.3 ± 1 W.

The experiment was repeated with a different measured input power of $P_{in}=35.9\pm1\,W$ that was determined from $\dot{T}(t)$ recorded on the krypton plasma as shown in Figure 21. From $\dot{T}(t)$ recorded on the helium-hydrogen (90/10%) plasma at the same input power readings as the control, also shown in Figure 21, the output and excess powers were determined to be 59.2 ± 1 W and 23.3 ± 1 W, respectively.

The sources of error were the error in the calibration curve (± 0.05 W) and the measured microwave input power (± 1 W). The propagated error of the calibration and power measurements was ± 1 W.

Given a helium-hydrogen (90/10%) flow rate of 10.0 sccm and an excess power of 24 W, energy balances of over $-3\,X\,10^{4}\,kJ/mole\,H_2$ ($150\,eV/H\,atom$) were measured. The reaction of hydrogen to form water which releases $-241.8\,kJ/mole\,H_2$ ($1.48\,eV/H\,atom$) is about 100 times less than that observed. Given that no conventional chemical reaction is plausible, the results indicate that the catalytic reaction of atomic

hydrogen with He^+ and subsequent autocatalytic reactions given previously [17, 19] occur to a significant extent. This is consistent with the previously reported series of lower-energy hydrogen lines with energies of $q \cdot 13.6\,eV$ where $q = 1,2,3,4,6,7,8,9, or\ 11$ [16-17, 19], the previously given theory [13-19], and previous studies which show very large energy balances [16-17].

c. MKS/Astex plasma discharge cell power balance measurements

Thermal power was primarily removed from the applicator by water cooling with minor heat loss from the applicator body to ambient and a negligible loss to the flowing test gas. For a microwave power input of about 1500 W, the gas exit temperature never exceeded inlet temperature by more than about 70°C for a flow rate of 50 sccm corresponding to an applicator-to-gas-stream power loss of less than 100 mW. In Figure 22, measured coolant power absorption is plotted versus microwave power input to the applicator for a helium plasma at 1 Torr and 50 sccm. There was excellent thermal coupling between the plasma and the cooling water as evidenced by the close tracking of the coolant enthalpy to the microwave power applied to the applicator. Thermal losses from the applicator to the ambient gradually increased with power input to about 8% for a power input of 1410 W. Degradation of thermal coupling between the plasma and coolant with increasing power may have resulted from elongation of the plasma in the quartz tube at high power levels. It was observed that when the plasma extended axially beyond the boundaries of the water-cooled plasma tube, thermal coupling was diminished.

In Figure 23, the water cooling temperature rise is plotted for varying helium plasma pressures at a fixed microwave power input of 1000 W. The power absorption by the cooling water for fixed power input was relatively insensitive to plasma pressure since the absorption decreased by only about 2.5% for a gas pressure below approximately 2 Torr. This behavior was also consistent with the greater thermal coupling between the coolant and plasma for higher pressure plasmas since they were more concentrated in the central zone of the applicator, coincident

with the cooling coil axial span.

The coolant temperature rise as a function of microwave power input to the applicator for helium, helium/hydrogen, xenon, and xenon/hydrogen plasmas at 1 Torr pressure and flow rates from 10 to 50 sccm is shown in Figure 24. To within the scatter in the data, the water temperature rise (and therefore the power absorption by the water) was the same for the helium-hydrogen plasmas as for the helium, xenon, and xenon-hydrogen control plasmas. The thermal power absorbed by the water stream for all these plasmas was only a few percent smaller than the microwave power input as shown in Figure 22.

d. Inductively coupled RF plasma discharge cell power balance measurements

The results of the measurement of the power balance on the RF cell are given in Table 4. The $T(t)$ water bath response was recorded with stirring alone and then with the selected panel meter reading of 40 W forward and 0 W reflected RF input power to krypton. Using the corresponding $\dot{T}(t)$ in Eq. (10), the RF input power was absolutely determined to be 37.0 ± 0.5 W. A helium-hydrogen (95/5%) mixture was run at the same RF input power readings as the control which corresponded to $P_{in} = 37.0 \pm 0.5\ W$ in Eq. (4). The $T(t)$ response was slightly increased for helium-hydrogen (95/5%). The output power given in Table 4 was determined to be 40.5 ± 0.5 W from the corresponding $\dot{T}(t)$ using Eq. (10). From Eq. (4), the excess power was 3.5 ± 0.5 W.

The experiment was repeated with the same measured input power of $P_{in} = 37.0 \pm 0.5\ W$. From $\dot{T}(t)$ recorded on the second helium-hydrogen (95/5%) plasma, the output and excess powers were determined to be 40.3 ± 1 W and 3.3 ± 1 W, respectively.

The sources of error were the error in the calibration curve (± 0.05 W) and the measured RF input power (± 0.5 W). The propagated error of the calibration and power measurements was ± 0.5 W.

IV. Discussion

A comparison of the different light sources for helium hydrogen

plasmas is given in Table 1. If the electric field was the source of the broadening, then the discharge cell would be anticipated to show the greatest broadening since the electric field in the cathode fall region was at least $1\,kV/cm$. Whereas, essentially no broadening would be expected from the microwave plasmas since no high field was present. The broadening observations were counter to the electric field relationship.

The results of the Langmuir probe measurements for the electron density n_e for the MKS/Astex discharge, inductively coupled RF, and microwave plasma cells were 10^{10}-$10^{11}\,cm^{-3}$ (measured), 10^{9}-$10^{11}\,cm^{-3}$ [7], $10^{9}\,cm^{-3}$ [29], and $<10^{9}\,cm^{-3}$ (measured), respectively. The electron density measurements by Langmuir probe shows that the trend in electron density was discharge > inductively coupled RF cell > microwave. Whereas, the trend in broadening of the Balmer α line was the opposite. No power or voltage dependence of the broadening was observed for any of the plasma sources studied. Neither the electron Stark effect nor any of the other conventional broadening mechanisms discussed previously [7-12, 20-21] can explain these results.

Excessive line broadening was only observed in the cases where an ion was present which could provide a net enthalpy of reaction of an integer multiple of the potential energy of atomic hydrogen (He^{+}). Whereas plasmas of chemically similar controls that do not provide gaseous atoms or ions that have electron ionization energies which are a close match to a multiple of $27.2\,eV$ (xenon or its ions) showed no broadening compared to pure hydrogen. These support the rt-plasma mechanism.

The power balance of the Evenson helium-hydrogen microwave plasma confirmed the presence of the exothermic reaction that corresponded to the significant broadening of 180-$210\,eV$. In contrast, no power was observed from the MKS/Astex system corresponding to the absence of broadening. The Evenson cavity has an E-mode [26-27]; whereas, the mode in the MKS/Astex is TM_{010}. We had shown previously that the conditions of the particular discharge may be a major parameter in the observation of excessive Doppler Balmer line broadening with plasmas of hydrogen and a noble ion having an ionization potential of an integer multiple of $27.2\,eV$ [20-21]. In addition, the comparison of Balmer and Lyman inverted populations with oxygen as the catalyst [30-31] in

different cavities indicates that the mode of the electromagnetic field is an important factor. The power density is also a factor as demonstrated by the weak inversion achieved in the TM_{010} MKS/Astex cavity with 10 times higher power input than the Evenson cavity as shown previously [32]. It was also observed that the Evenson microwave cavity with appropriate tuning discussed previously [33] provides favorable conditions for the catalytic reaction of He^+ with atomic hydrogen.

Relatively low levels of power from the glow discharge cell matched the single population with a lower H energy than the Evenson microwave cell. The lower power level compared to the Evenson microwave cell was consistent with the absence of population inversion and the inferiority of the discharge light source for producing the novel series of lines of energies $q \cdot 13.6\,eV$ ($q = 1,2,3,4,6,7,8,9,$ *or* 11) or these energies less $21.2\,eV$ due to inelastic scattering of the lines by helium atoms in the excitation of $He\,(1s^2)$ to $He\,(1s^1 2p^1)$ observed with the Evenson microwave cell [30-34].

The inductively coupled RF cell showed significant broadening, but only minor excess power. This may be due to the existence of only a small population with significant energy. The absence of significant power was consistent with the absence of population inversion and the inferiority of the RF light source for producing the novel series of lines of energies $q \cdot 13.6\,eV$ [30-34].

The broadening and power results were also consistent with the observation of the novel series $E_{D+vib} = 4^2 E_{D H_2^+} \pm \upsilon^* 2^2 E_{vib H_2^+(\upsilon=0\rightarrow\upsilon=1)}$ at the longer wavelengths for $\upsilon^* = 0$ to $\upsilon^* = 20$ and at the shorter wavelengths for $\upsilon^* = 0$ to $\upsilon^* = 3$ where $E_{D H_2^+}$ and $E_{vib H_2^+(\upsilon=0\rightarrow\upsilon=1)}$ are the experimental bond and vibrational energies of H_2^+, respectively [35]. The vibrational series was observed for helium only with the Evenson microwave or glow discharge cell, but not with the inductively coupled RF cell. The microwave cell consistently produced the most intense lines [35].

IV. SUMMARY AND CONCLUSIONS

Line broadening of the hydrogen Balmer lines provides a sensitive measure of the number and energy of excited hydrogen atoms in different plasma sources. From the width of the 656.3 nm Balmer α line

emitted from glow discharge, Evenson microwave, MKS/Astex microwave, and inductively coupled RF plasmas, it was found that Evenson cavity microwave helium-hydrogen plasmas showed significant broadening corresponding to an average hydrogen atom energy of 180-210 eV with only a fast population. Inductively coupled RF helium-hydrogen plasmas showed extraordinary broadening corresponding to an average hydrogen atom energy of 250−310 eV, but the fast population was a minor component compared to the slow of $\approx 35\,eV$ and the volume of energetic H was small and very plasma condition dependent. The corresponding results from the glow discharge plasmas were 33-38 eV and 30-35 eV, respectively, compared to $\approx 4\,eV$ for plasmas of pure hydrogen and xenon-hydrogen maintained in any of the sources and helium-hydrogen plasmas maintained in the MKS/Astex microwave system.

Excessive line broadening was only observed for the ions which provided a net enthalpy of reaction of a multiple of the potential energy of the hydrogen atom. The electron density was far too low for detectable Stark broadening, and the trend in n_e was opposite that of the broadening. And, no high electric field was present in the microwave plasmas. Thus, the results can not be explained by external Stark broadening or acceleration of charged species due to high fields of over $10\,kV/cm$ as proposed by Videnovic et al. [8] to explain excessive broadening observed in glow discharges. Similarly, previous explanations based on field acceleration of ions at the powered electrode of RF cells are insufficient [7-12, 20-21]. The results are consistent with an energetic reaction caused by a resonant energy transfer between hydrogen atoms and He^+ as the source of the excessive line broadening. Considering the volume, population densities, and energies of fast H, the reaction rate was higher under the conditions of an Evenson microwave compared to glow discharge, MKS/Astex microwave, and inductively coupled RF plasmas even at a lower input power.

The corresponding exothermic reaction was confirmed by power balance measurements. With an input of 24.8± 1 W, the total plasma power of the Evenson microwave helium-hydrogen plasma measured by water bath calorimetry was 49.1 ± 1 W corresponding to 24.3 ± 1 W of excess power in 3 cm^3. The excess power density and energy balance were high, 8.1 W/cm^3 and over $-3\,X\,10^4\,kJ/mole\,H_2$, respectively. With an

input of 500 W, a total power of 623 W was generated in a 45 cm^3 compound-hollow-cathode-glow discharge. Less than 10% excess power was observed from inductively coupled RF helium-hydrogen plasmas. No measurable heat was observed from MKS/Astex microwave helium-hydrogen plasmas.

REFERENCES

1. P. W. J. M. Boumans, Spectrochim. Acta Part B, 46 (1991) 711.
2. J. A. C. Broekaert, Appl. Spectrosc., 49, (1995) 12A.
3. P. W. J. M. Boumans, J. A. C. Broekaert, and R. K. Marcus, Eds., Spectrochim. Acta Part B, 46 (1991) 457.
4. M. Dogan, K. Laqua, and H. Massmann, "Spektrochemische Analysen mit einer Glimmentladungslampe als Lichtquelle—I," Spectrochim. Acta, Volume 26B, (1971) 631–649.
5. M. Dogan, K. Laqua, and H. Massmann, "Spektrochemische Analysen mit einer Glimmentladungslampe als Lichtquelle—II, "Spectrochim. Acta, Volume 27B, (1972) 65–88.
6. J. A. C. Broekaert, J. Anal. At. Spectrom., 2 (1987) 537.
7. M. Kuraica, N. Konjevic, "Line shapes of atomic hydrogen in a plane-cathode abnormal glow discharge", Physical Review A, Volume 46, No. 7, October (1992), pp. 4429-4432.
8. I. R. Videnovic, N. Konjevic, M. M. Kuraica, "Spectroscopic investigations of a cathode fall region of the Grimm-type glow discharge", Spectrochimica Acta, Part B, Vol. 51, (1996), pp. 1707-1731.
9. S. Alexiou, E. Leboucher-Dalimier, "Hydrogen Balmer-α in dense plasmas", Phys, Rev. E, Vol. 60, No. 3, (1999), pp. 3436-3438.
10. S. Djurovic, J. R. Roberts, "Hydrogen Balmer alpha line shapes for hydrogen -argon mixtures in a low-pressure rf discharge", J. Appl. Phys., Vol. 74, No. 11, (1993), pp. 6558-6565.
11. S. B. Radovanov, K. Dzierzega, J. R. Roberts, J. K. Olthoff, Time-resolved Balmer-alpha emission from fast hydrogen atoms in low pressure, radio-frequency discharges in hydrogen", Appl. Phys. Lett., Vol. 66, No. 20, (1995), pp. 2637-2639.
12. S. B. Radovanov, J. K. Olthoff, R. J. Van Brunt, S. Djurovic, "Ion kinetic-energy distributions and Balmer-alpha (H_α) excitation in $Ar-H_2$ radio-

frequency discharges", J. Appl. Phys., Vol. 78, No. 2, (1995), pp. 746-757.
13. R. Mills and M. Nansteel, P. Ray, "Argon-Hydrogen-Strontium Discharge Light Source", IEEE Transactions on Plasma Science, Vol. 30, No. 2, (2002), pp. 639-653.
14. R. Mills, J. Dong, Y. Lu, "Observation of Extreme Ultraviolet Hydrogen Emission from Incandescently Heated Hydrogen Gas with Certain Catalysts", Int. J. Hydrogen Energy, Vol. 25, (2000), pp. 919-943.
15. R. Mills and M. Nansteel, P. Ray, "Bright Hydrogen-Light Source due to a Resonant Energy Transfer with Strontium and Argon Ions", New Journal of Physics, Vol. 4, (2002), pp. 70.1-70.28.
16. R. L. Mills, P. Ray, B. Dhandapani, M. Nansteel, X. Chen, J. He, "Spectroscopic Identification of Transitions of Fractional Rydberg States of Atomic Hydrogen", J. of Quantitative Spectroscopy and Radiative Transfer, in press.
17. R. L. Mills, P. Ray, B. Dhandapani, M. Nansteel, X. Chen, J. He, "New Power Source from Fractional Quantum Energy Levels of Atomic Hydrogen that Surpasses Internal Combustion", J Mol. Struct., Vol. 643, No. 1-3, (2002), pp. 43-54.
18. R. Mills, "Spectroscopic Identification of a Novel Catalytic Reaction of Atomic Hydrogen and the Hydride Ion Product", Int. J. Hydrogen Energy, Vol. 26, No. 10, (2001), pp. 1041-1058.
19. R. Mills, P. Ray, "Spectral Emission of Fractional Quantum Energy Levels of Atomic Hydrogen from a Helium-Hydrogen Plasma and the Implications for Dark Matter", Int. J. Hydrogen Energy, Vol. 27, No. 3, pp. 301-322.
20. R. L. Mills, P. Ray, B. Dhandapani, R. M. Mayo, J. He, "Comparison of Excessive Balmer α Line Broadening of Glow Discharge and Microwave Hydrogen Plasmas with Certain Catalysts", J. of Applied Physics, (2002), Vol. 92, No. 12, pp. 7008-7022.
21. R. L. Mills, P. Ray, E. Dayalan, B. Dhandapani, J. He, "Comparison of Excessive Balmer α Line Broadening of Inductively and Capacitively Coupled RF, Microwave, and Glow Discharge Hydrogen Plasmas with Certain Catalysts", IEEE Transactions on Plasma Science, in press.
22. J. Tadic, I. Juranic, G. K. Moortgat, "Pressure dependence of the photooxidation of selected carbonyl compounds in air: n-butanal and

n-pentanal", J. Photochemistry and Photobiology A: Chemistry, Vol. 143, (2000), 169-179.
23. H. R. Griem, *Principles of Plasma Spectroscopy*, Cambridge University Press, (1997).
24. G. Sultan, G. Baravian, M. Gantois, G. Henrion, H. Michel, A. Ricard, "Doppler-broadened H_α line shapes in a dc low-pressure discharge for *TiN* deposition", Chemical Physics, Vol. 123, (1988), pp. 423-429.
25. F. F. Chen, "Electric Probes", in Plasma Diagnostic Techniques, R. H. Huddleston and S. L. Leonard, Eds., Academic Press, NY, (1965).
26. F. C. Fehsenfeld, K. M. Evenson, H. P. Broida, "Microwave discharges operating at 2450 MHz", Review of scientific Instruments, Vol. 35, No. 3, (1965), pp. 294-298.
27. B. McCarroll, "An improved microwave discharge cavity for 2450 MHz", Review of Scientific Instruments, Vol. 41, (1970), p. 279.
28. N. V. Sidgwick, *The Chemical Elements and Their Compounds*, Volume I, Oxford, Clarendon Press, (1950), p.17.
29. D. Barton, J. W. Bradley, D. A. Steele, and R. D. Short, "investigating radio frequency plasmas used for the modification of polymer surfaces," J. Phys. Chem. B, Vol. 103, (1999), pp. 4423-4430.
30. R. Mills, P. Ray, R. M. Mayo, "The Potential for a Hydrogen Water-Plasma Laser", Applied Physics Letters, Vol. 82, No. 11, (2003), pp. 1679-1681.
31. R. Mills, P. Ray, R. M. Mayo, "Stationary Inverted Balmer and Lyman Populations for a CW HI Water-Plasma Laser", IEEE Transactions on Plasma Science, submitted.
32. R. Mills, P. Ray, M. Nansteel, R. M. Mayo, "Comparison of Water-Plasma Sources of Stationary Inverted Balmer and Lyman Populations for a CW HI Laser", J. Appl. Spectroscopy, New Journal of Physics, submitted.
33. R. L. Mills, P. Ray, B. Dhandapani, J. He, "Energetic Helium-Hydrogen Plasma Reaction", AIAA Journal, submitted.
34. R. L. Mills, P. Ray, B. Dhandapani, X. Chen, "Comparison of Catalysts and Microwave Plasma Sources of Spectral Emission of Fractional-Principal-Quantum-Energy-Level Atomic and Molecular Hydrogen", Journal of Applied Spectroscopy, submitted.
35. R. Mills, J. He, A. Echezuria, B Dhandapani, P. Ray, "Comparison of Catalysts and Plasma Sources of Vibrational Spectral Emission of

Fractional-Rydberg-State Hydrogen Molecular Ion", European Journal of Physics D, submitted.

Table 1. The comparison of the energies of the slow and fast atoms of hydrogen, xenon-hydrogen (90/10%), and helium-hydrogen (90/10%) glow discharge, Evenson microwave cavity, MKS/Astex microwave system, and inductively coupled RF plasmas.

Plasma System	Hydrogen Atom Energy[a] (eV) ($\pm 5\%$)			
	Pure H_2	Xe/H_2	He/H_2	
			Slow	Fast
Glow Discharge	3 - 4	3 - 4		35 - 40
Evenson Microwave Cavity	3 - 5	3 - 5		180 - 210
MKS/Astex Microwave System	1 - 2	1 - 2	3 - 5	
Inductively Coupled RF Cell	3 - 5	3 - 5	35 - 40	250 - 310

[a] Calculated after [8, 20]

Table 2. Temperature rise variation with power input to the calibration heater.

Input Power (W)	Voltage (V)	Current (A)	Temp. Rise Above 200.0 °C ΔT ($\pm 0.1\,°C$)
100	32.4	3.088	67.3
200	49.2	4.065	118.9
300	65.3	4.60	162.7
400	82.5	4.85	198.4

Table 3. The total output power and excess power at selected input powers for the helium-hydrogen glow discharge plasma.

Input Power (W)	Voltage (V)	Current (A)	Temp. Rise Above 200.0 °C ΔT ($\pm 0.1\ ^{\circ}C$)	Total Output Power P_{out} ($\pm 5\ W$) Eq. (8)	Excess Power P_{ex} ($\pm 5\ W$) Eq. (9)
100	327	0.306	67.3	100.1	0.1
200	313	0.639	130.8	225.1	25.1
300	305	0.984	186.9	366.4	66.4
400	308	1.299	226.9	488.1	88.1
500	310	1.613	265.2	623.2	123.2

Table 4. The total output power and excess power of helium-hydrogen RF discharge plasmas at an input power matched with a control xenon discharge plasma.

Plasma gas	Input Power (W))[a]	Total Output Power P_{out} ($\pm 0.5\ W$) Eq. (10)	Excess Power P_{ex} ($\pm 0.5\ W$) Eq. (4)
Xe	37.0	37.0	0.0
$He/H_2(5\%)$	37.0	40.5	3.5
$He/H_2(5\%)$	37.0	40.3	3.3

[a] The reflected power was zero.

Figure Captions

Figure 1. Cylindrical stainless steel cell for studies of the broadening of the Balmer α line emitted from glow discharge plasmas of pure hydrogen alone and a mixture of 10% hydrogen and helium or xenon.

Figure 2. The experimental set up comprising a Evenson cavity microwave discharge cell light source.

Figure 3. The experimental set up comprising an MKS/Astex microwave system light source. Power was delivered to the plasma applicator through a waveguide system comprising a microwave power generator and magnetron, circulator, and stub tuner.

Figure 4. Schematic of the MKS/Astex water flow calorimeter. The MKS/Astex microwave plasma applicator comprised a 25 mm quartz tube housed concentrically within a cylindrical cavity and oriented normal to the axis of a rectangular waveguide. The copper tubing was bonded to the outer surface of the quartz tube that permitted excellent thermal coupling between the plasma and the coolant stream. The inlet and outlet coolant temperature and the constant flow rate permitted the power balance to be determined to within ±3%.

Figure 5. The experimental set up comprising a inductively coupled RF cell light source.

Figure 6. Cylindrical stainless steel glow discharge cell and the compound hollow cathode used for power balance studies.

Figure 7. The experimental setup for generating a glow discharge plasma and for measuring the power balance.

Figure 8. Schematic of the Evenson microwave cavity water bath calorimeter. The Evenson cavity and a plasma-containing section of the quartz tube were fitted with a water-tight stainless steel housing, and the housing and cell assembly were suspended by 4 support rods from an acrylic plate which held the cell vertically from the top of a water bath calorimeter.

Figure 9. The 656.3 nm Balmer α line width recorded with a high resolution ($\pm 0.025\,nm$) visible spectrometer on a xenon-hydrogen (90/10%) and a hydrogen glow discharge plasma. No excessive line broadening was observed corresponding to an average hydrogen atom energy of $3-4\,eV$.

Figure 10. The 656.3 nm Balmer α line width recorded with a high resolution ($\pm 0.025\,nm$) visible spectrometer on a helium-hydrogen (90/10%) and a hydrogen glow discharge plasma. Significant broadening was observed corresponding to an average hydrogen atom energy of $33-38\,eV$.

Figure 11. The 656.3 nm Balmer α line width recorded with a high resolution ($\pm 0.006\,nm$) visible spectrometer on a xenon-hydrogen (90/10%) and a hydrogen Evenson microwave discharge plasma. No excessive line broadening was observed corresponding to an average hydrogen atom energy of $3-5\,eV$.

Figure 12. The 656.3 nm Balmer α line width recorded with a high resolution ($\pm 0.006\,nm$) visible spectrometer on a helium-hydrogen (90/10%) and a hydrogen Evenson microwave discharge plasma. Significant broadening was observed corresponding to an average hydrogen atom energy of $180-210\,eV$.

Figure 13. The 667.816 *nm He* I line width recorded with a high resolution ($\pm 0.006\,nm$) visible spectrometer on helium-hydrogen (90/10%) (solid curve) and helium (dotted curve) Evenson microwave discharge plasmas. No broadening was observed in either case.

Figure 14. The 656.3 nm Balmer α line width recorded radially with a high resolution ($\pm 0.006\,nm$) visible spectrometer on 1.5 kW-system MKS/Astex microwave discharge plasmas of hydrogen compared with helium-hydrogen (98/2%) with 150-1000 W input power at 0.5 and 1 Torr. The line broadening of the helium-hydrogen plasma was completely negligible at 150 W, but at 1000 W microwave input, the Balmer line width (FWHM) was broadened by about 0.1 and 0.3 Å compared with pure hydrogen for 0.5 and 1 Torr, respectively.

Figure 15. The 656.3 nm Balmer α line width recorded axially with a high resolution ($\pm 0.006\,nm$) visible spectrometer on 5 kW-system MKS/Astex microwave discharge plasmas of hydrogen compared with helium-hydrogen (98/2%) with 1000 W input power at 0.5 and 1 Torr. At 1000 W microwave input, the Balmer line width (FWHM) was broadened by about 0.5 and 0.9 Å compared with pure hydrogen for 1 and 0.5 Torr, respectively.

Figure 16. The 656.3 nm Balmer α line width recorded with a high resolution ($\pm 0.006\,nm$) visible spectrometer on a xenon-hydrogen

(90/10%) and a hydrogen inductively coupled RF plasma. No excessive line broadening was observed corresponding to an average hydrogen atom energy of $3-5\,eV$.

Figure 17. The 656.3 nm Balmer α line width recorded with a high resolution ($\pm 0.006\,nm$) visible spectrometer on an helium-hydrogen (90/10%) and a hydrogen inductively coupled RF plasma. Significant broadening was observed from a minor fast population corresponding to an average hydrogen atom energy of $250-310\,eV$.

Figure 18. The temperature increase above the constant kiln temperature of $200.0\,°C$ as a function of the power applied to each of the gas mixtures and a calibration heater. Significant excess power was observed in the case of helium-hydrogen glow discharge plasmas; whereas, no excess power was observed from krypton-hydrogen plasmas compared to the heater calibration.

Figure 19. The thermogram, $T(t)$ response of the cell, with stirring only and with a constant input power to the high precision heater of 50 W. The baseline corrected least squares fit of the slope, $\dot{T}(t)$, was $2.622\,X\,10^{-4}\,°C/s$, and the heat capacity was determined to be $1.907\,X\,10^{5}\,J/°C$.

Figure 20. The $T(t)$ water bath response to stirring and then with selected panel meter readings of the constant forward and reflected microwave input power to krypton was recorded. The microwave input power was determined to be 24.8± 1 W. A helium-hydrogen (90/10%) mixture was run at identical microwave input power readings as the control, and the excess power was determined to be 24.3 ± 1 W from the $T(t)$ response.

Figure 21. The $T(t)$ water bath response to stirring and then with selected panel meter readings of the constant forward and reflected microwave input power to krypton was recorded. The microwave input power was determined to be 35.9 ± 1 W. A helium-hydrogen (90/10%) mixture was run at identical microwave input power readings as the control, and the excess power was determined to be 23.3 ± 1 W from the $T(t)$ response.

Figure 22. Measured coolant power absorption in the Astex microwave applicator plotted versus microwave power input for a helium plasma at 1 Torr and 50 sccm. There was excellent thermal coupling

between the plasma and the cooling water as evidenced by the close tracking of the coolant enthalpy to the microwave power applied to the applicator.

Figure 23. The water temperature rise plotted for varying helium plasma pressures at a fixed microwave power input of 1000 W to the Astex applicator. The power absorption by the cooling water for fixed power input was relatively insensitive to plasma pressure since the absorption decreased by only about 2.5% for a gas pressure below approximately 2 Torr.

Figure 24. The coolant temperature rise as a function of microwave power input to the Astex applicator for helium, helium/hydrogen, xenon, and xenon/hydrogen plasmas at 1 Torr pressure and flow rates from 10 to 50 sccm. To within the scatter in the data, the water temperature rise (and therefore the power absorption by the water) was the same for the helium-hydrogen plasmas as for the helium, xenon, and xenon-hydrogen control plasmas. No excess power was observed.

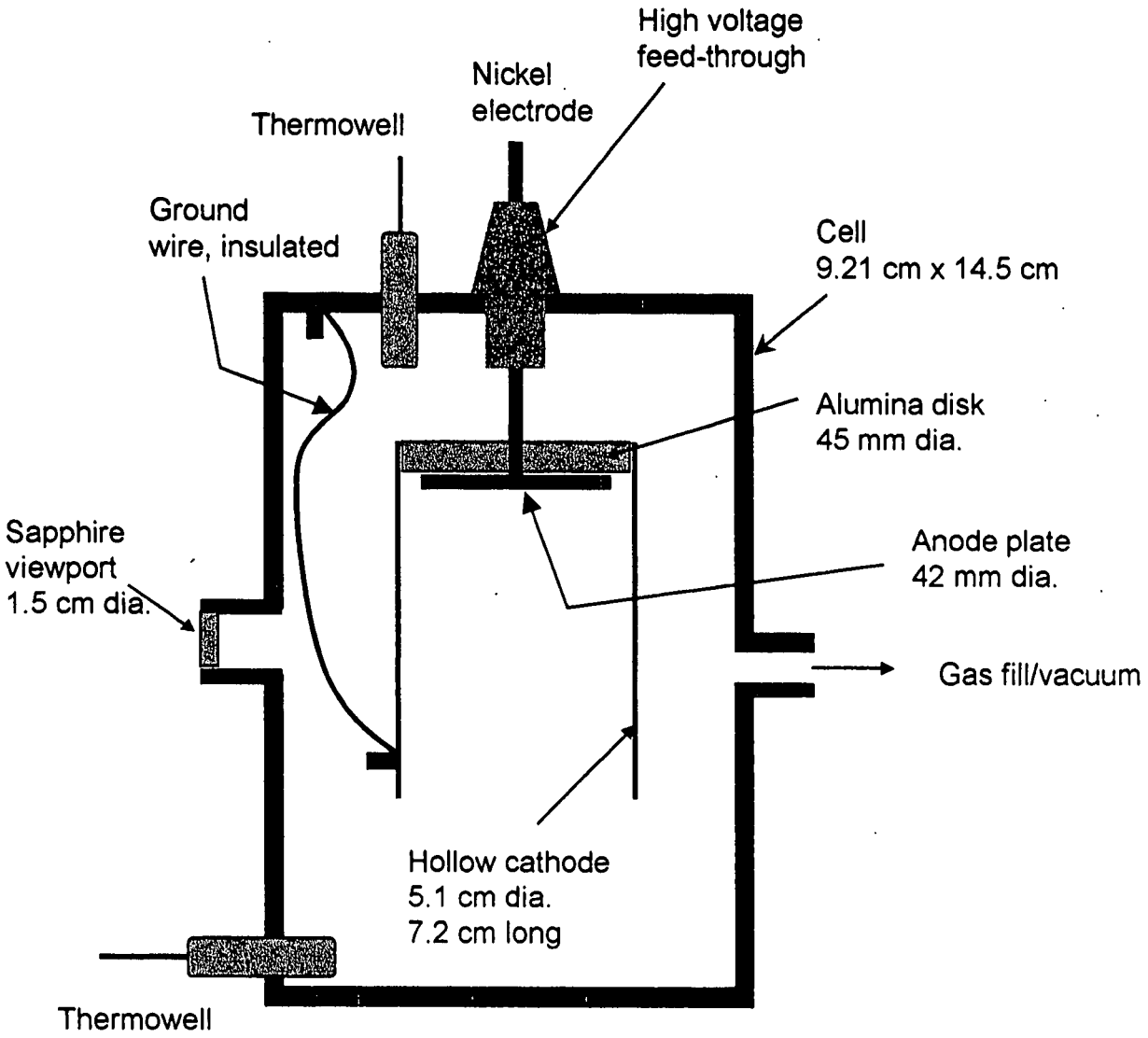
High voltage
feed-through
Nickel
electrode
Thermowell
Ground
wire, insulated
Cell
9.21 cm x 14.5 cm
Alumina disk
45 mm dia.
Sapphire
viewport
1.5 cm dia.
Anode plate
42 mm dia.
Gas fill/vacuum
Hollow cathode
5.1 cm dia.
7.2 cm long
Thermowell

Fig. 1

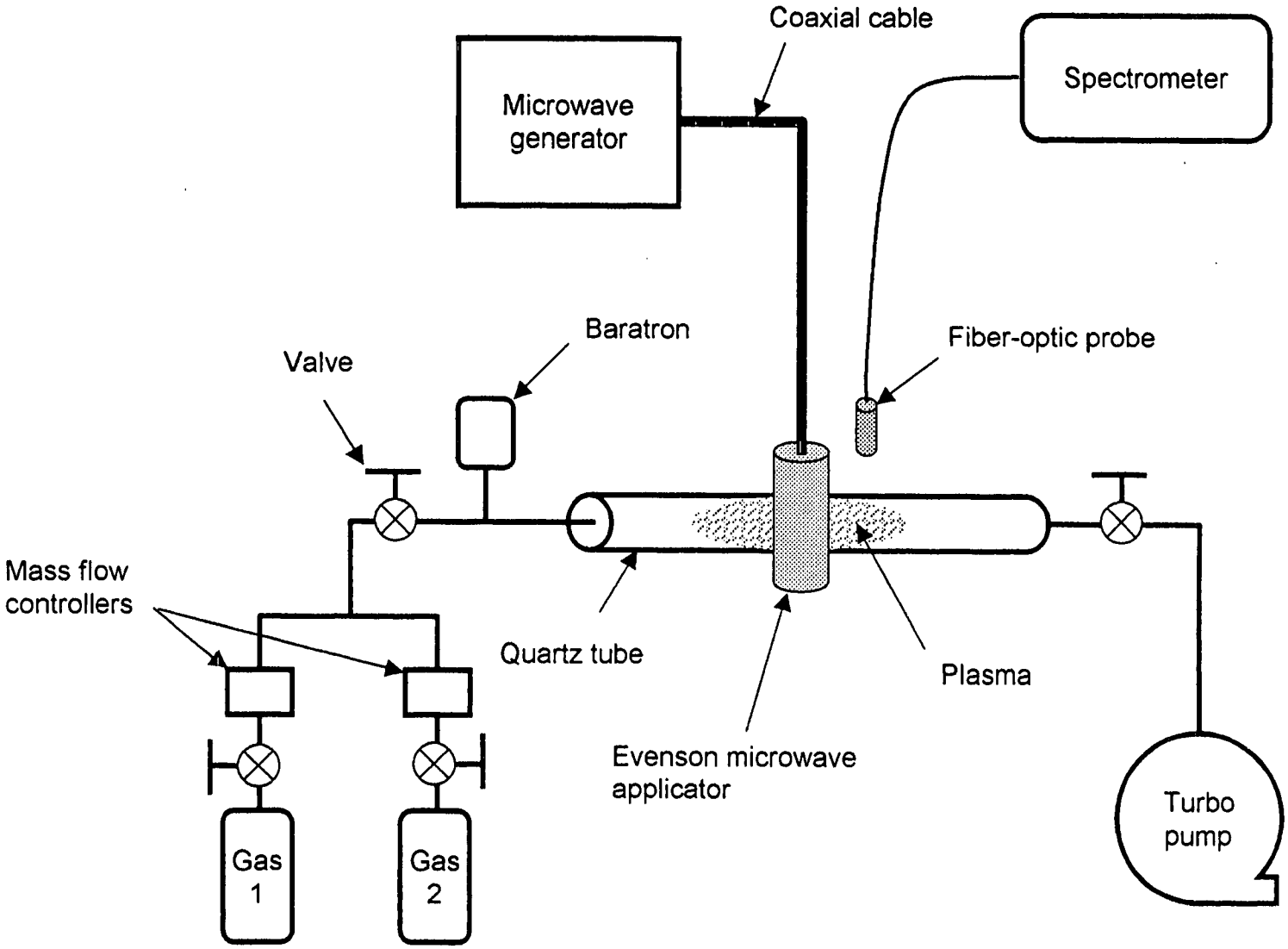
Coaxial cable
Microwave generator
Spectrometer
Baratron
Valve
Fiber-optic probe
Mass flow controllers
Quartz tube
Plasma
Evenson microwave applicator
Turbo pump
Gas 1
Gas 2

Fig. 2

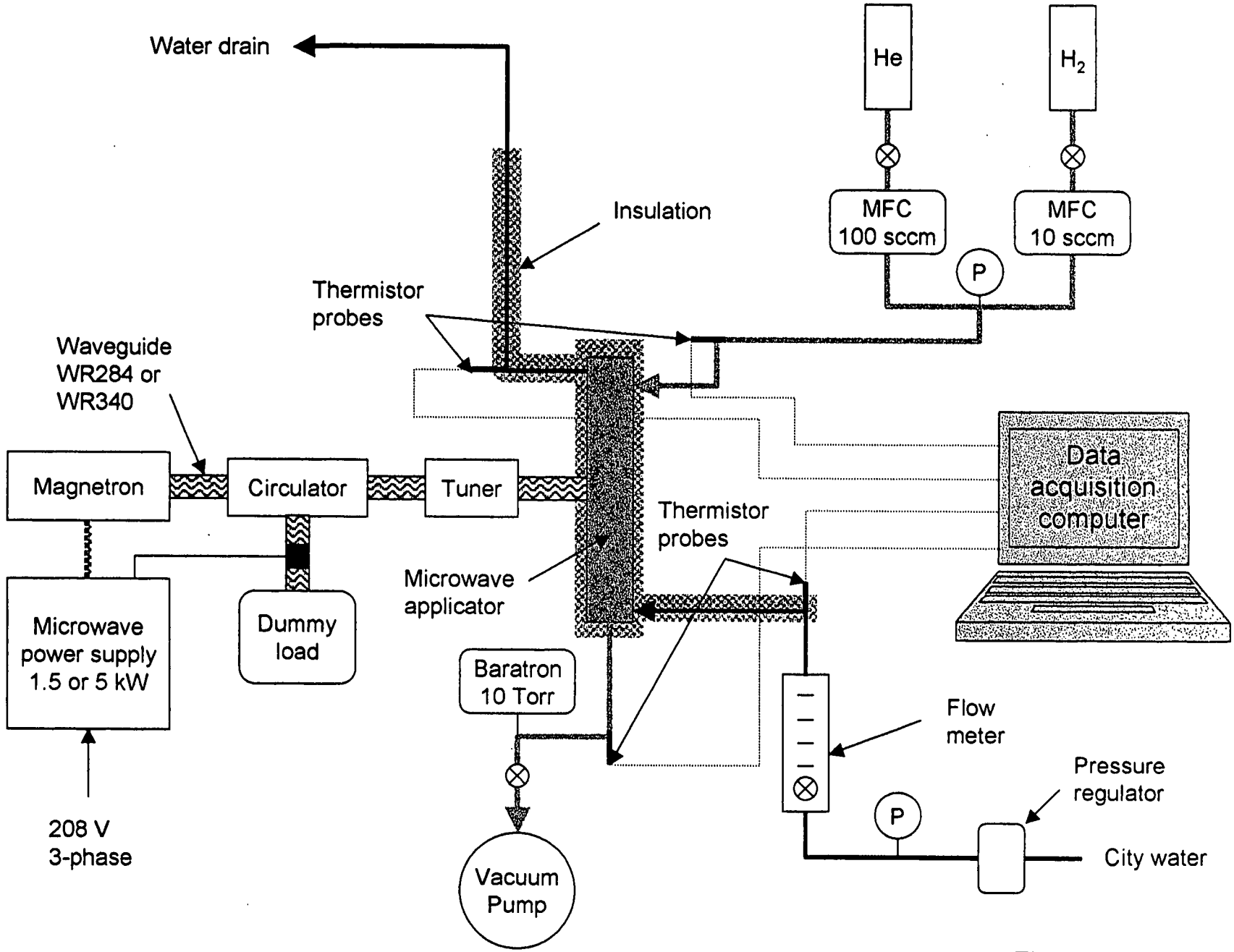
Water drain
He
H_2
MFC
100 sccm
MFC
10 sccm
P
Insulation
Thermistor
probes
Waveguide
WR284 or
WR340
Magnetron
Circulator
Tuner
Data
acquisition
computer
Thermistor
probes
Microwave
applicator
Microwave
power supply
1.5 or 5 kW
Dummy
load
Baratron
10 Torr
Flow
meter
Pressure
regulator
P
City water
208 V
3-phase
Vacuum
Pump

Fig. 3

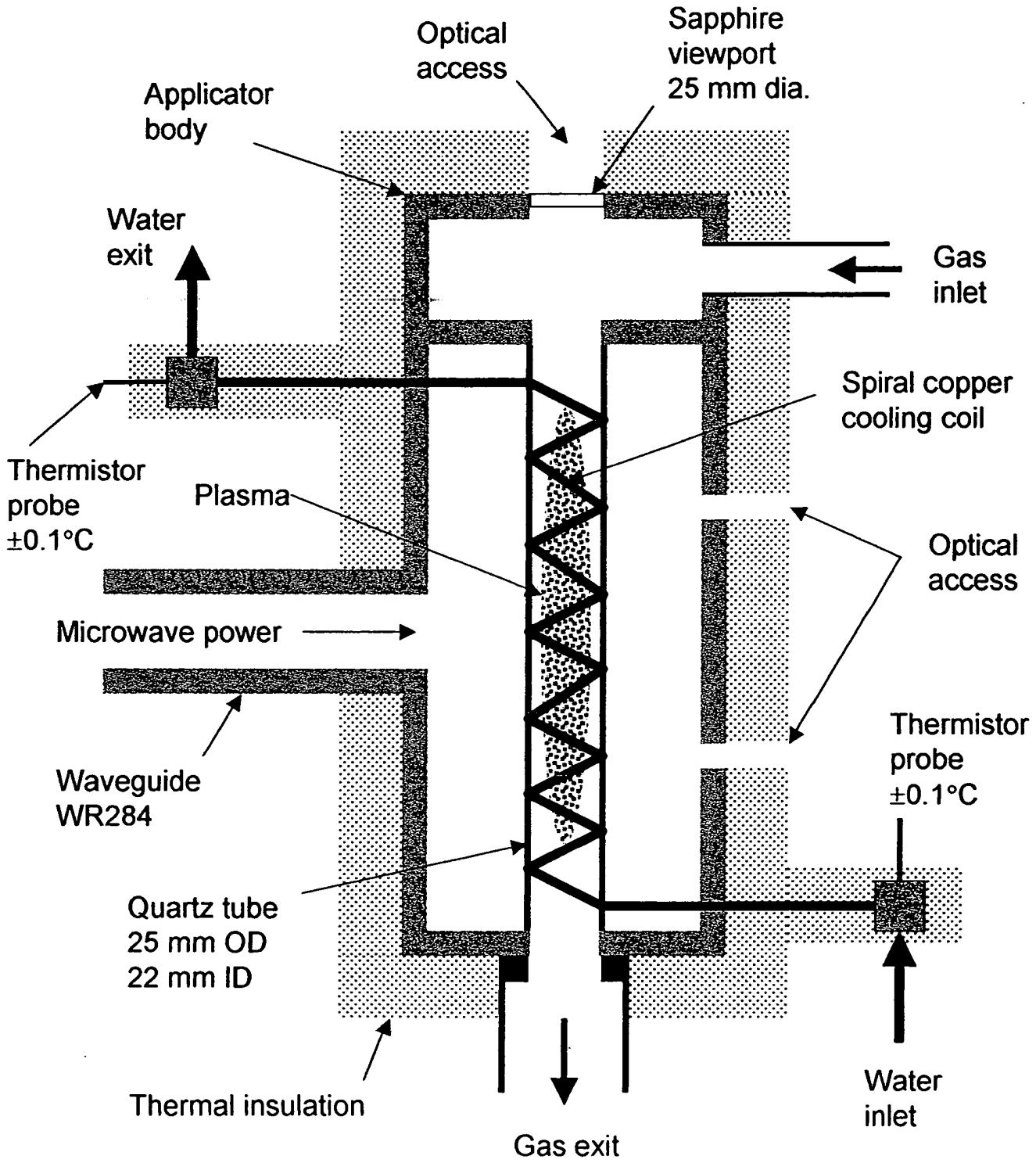
Optical access
Sapphire viewport 25 mm dia.
Applicator body
Water exit
Gas inlet
Spiral copper cooling coil
Thermistor probe ±0.1°C
Plasma
Optical access
Microwave power
Waveguide WR284
Thermistor probe ±0.1°C
Quartz tube 25 mm OD 22 mm ID
Thermal insulation
Water inlet
Gas exit

Fig. 4

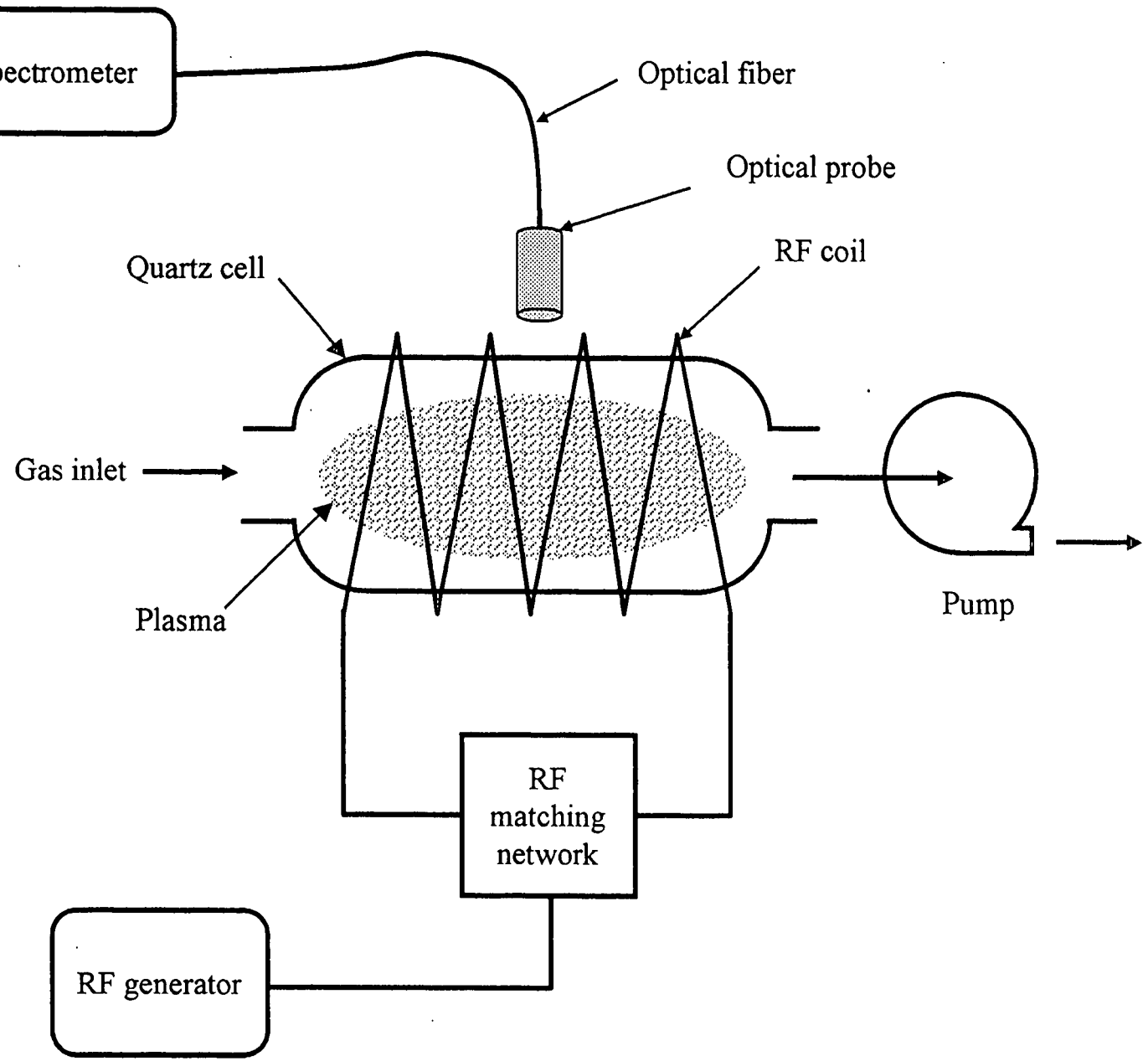
Spectrometer
Optical fiber
Optical probe
Quartz cell
RF coil
Gas inlet
Plasma
Pump
RF matching network
RF generator

Fig. 5

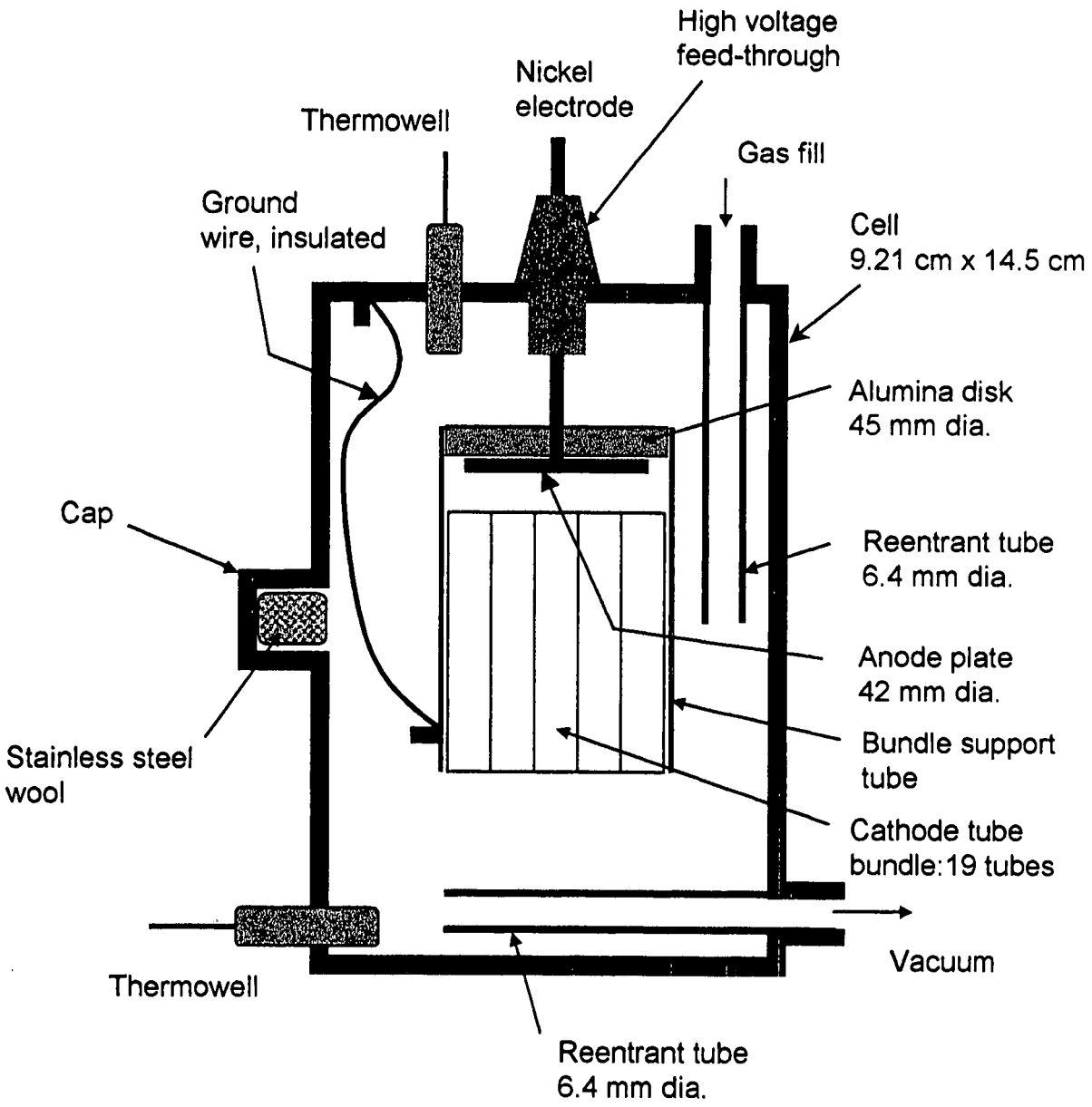
High voltage
feed-through
Nickel
electrode
Thermowell
Gas fill
Ground
wire, insulated
Cell
9.21 cm x 14.5 cm
Alumina disk
45 mm dia.
Cap
Reentrant tube
6.4 mm dia.
Anode plate
42 mm dia.
Stainless steel
wool
Bundle support
tube
Cathode tube
bundle:19 tubes
Vacuum
Thermowell
Reentrant tube
6.4 mm dia.

Fig. 6

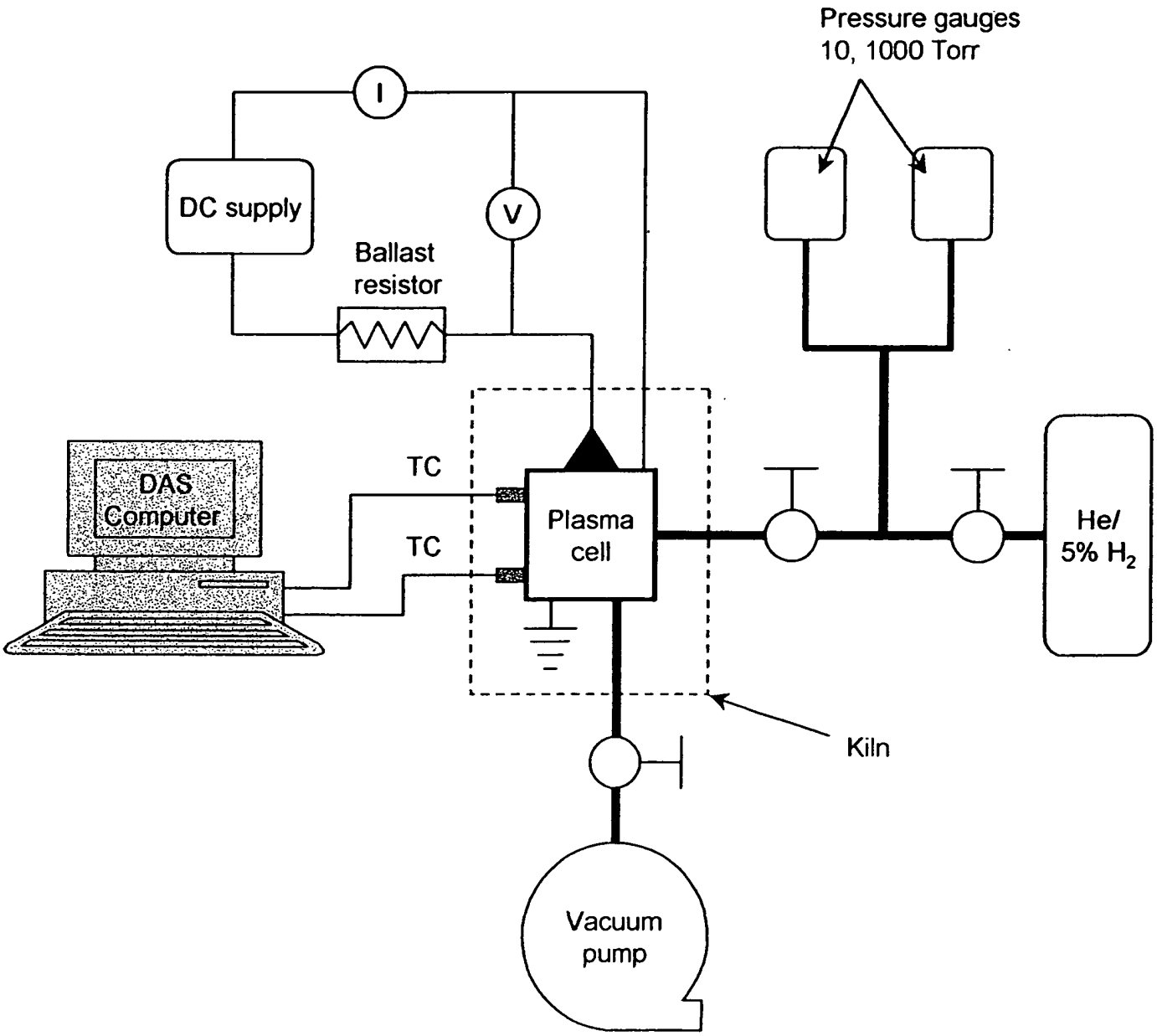
Pressure gauges
10, 1000 Torr
I
DC supply
V
Ballast
resistor
DAS
Computer
TC
TC
Plasma
cell
He/
5% H_2
Kiln
Vacuum
pump

Fig. 7

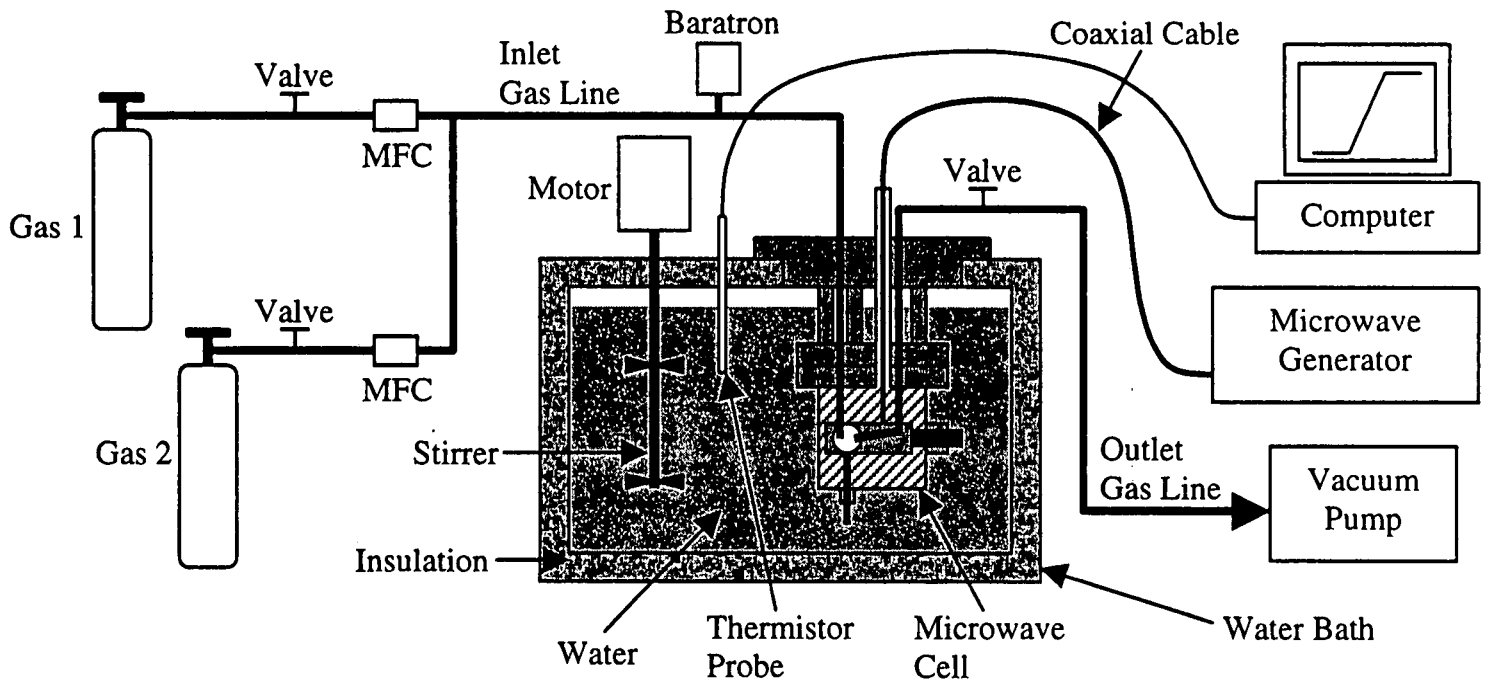
Baratron
Coaxial Cable
Valve
Inlet
Gas Line
MFC
Motor
Valve
Computer
Gas 1
Microwave
Generator
Valve
MFC
Gas 2
Stirrer
Outlet
Gas Line
Vacuum
Pump
Insulation
Water
Thermistor
Probe
Microwave
Cell
Water Bath

Fig. 8

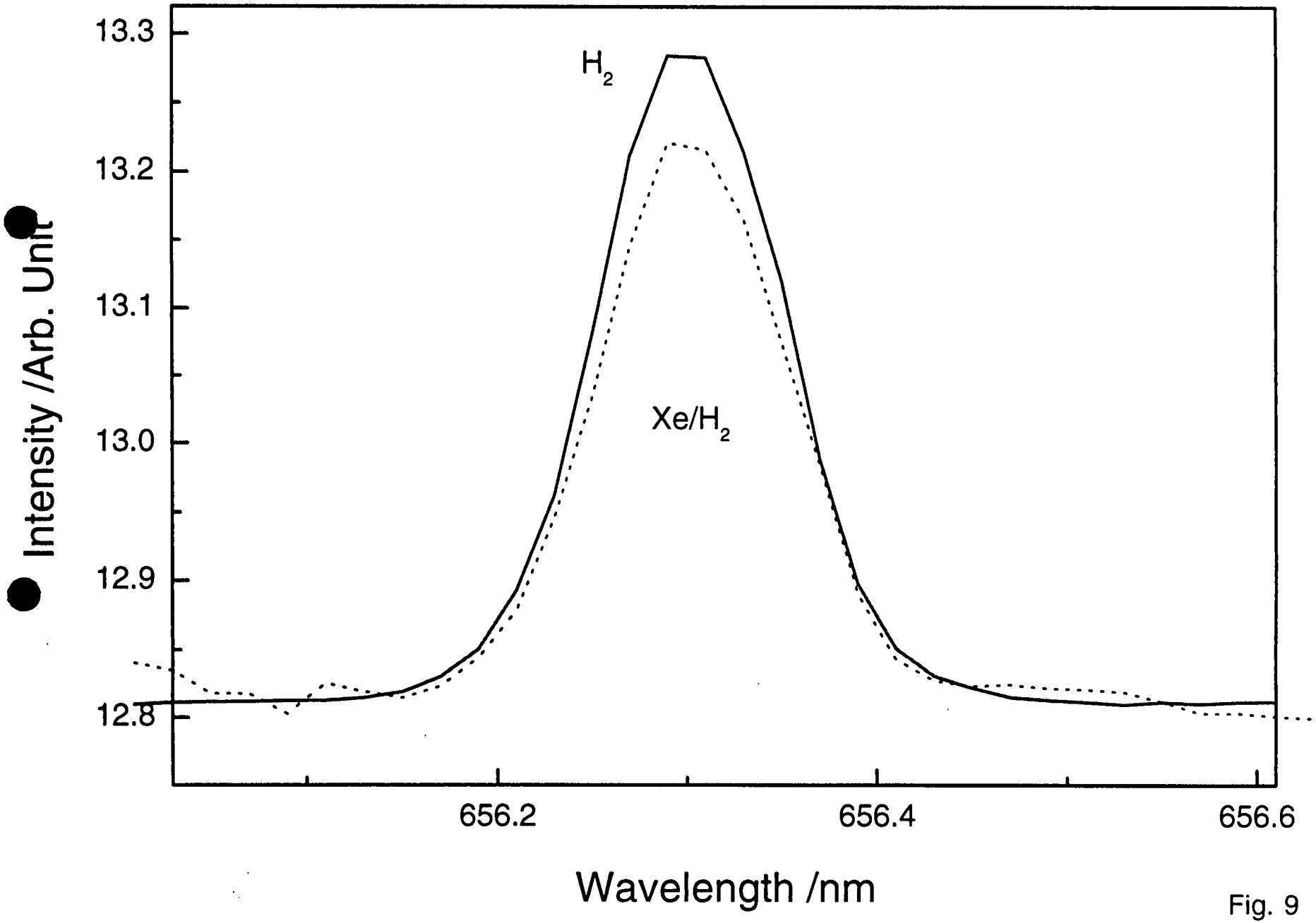
13.3
13.2
13.1
13.0
12.9
12.8
Intensity /Arb. Unit
H2
Xe/H2
656.2
656.4
656.6
Wavelength /nm

Fig. 9

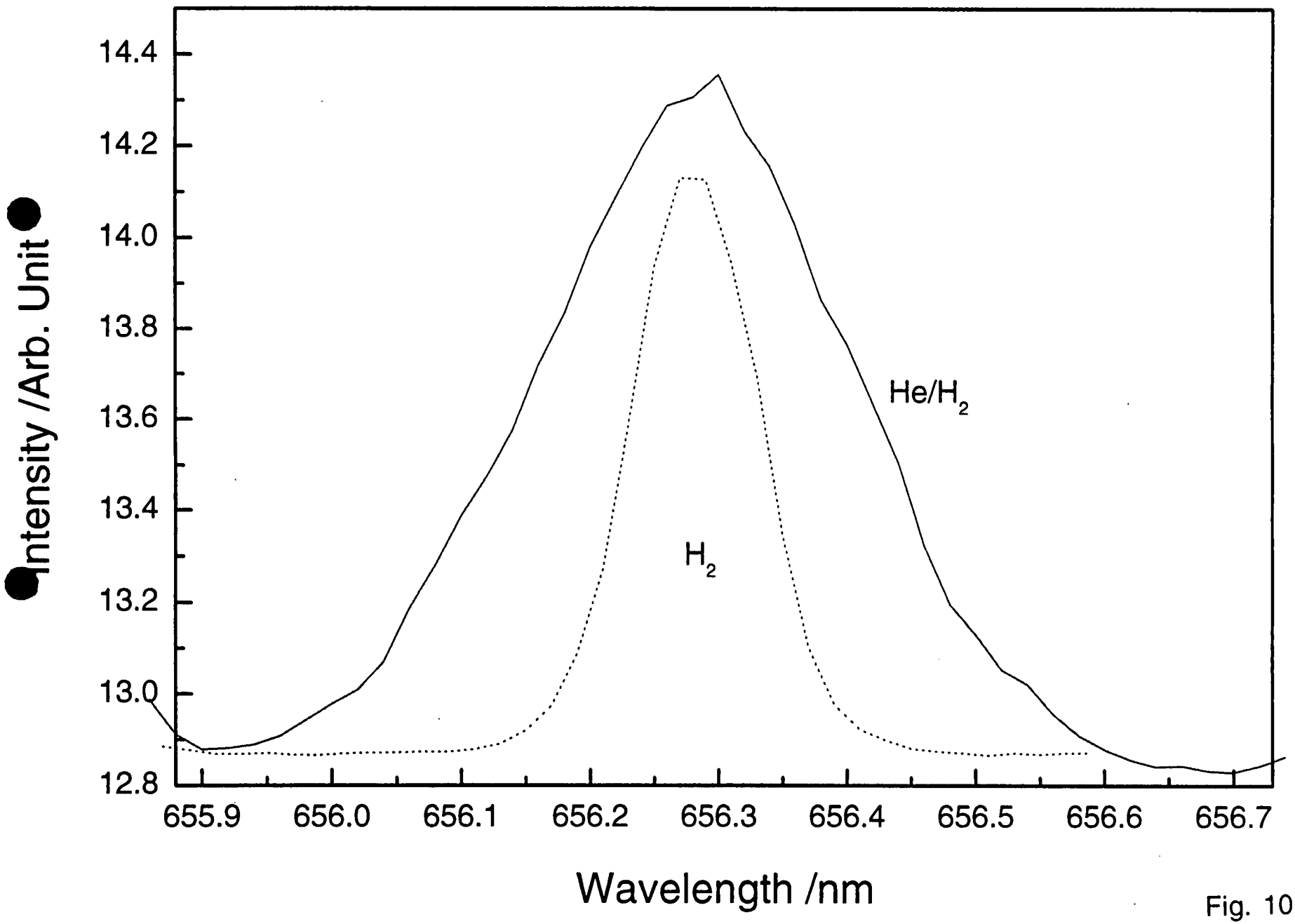
Intensity /Arb. Unit
14.4
14.2
14.0
13.8
13.6
13.4
13.2
13.0
12.8
He/H2
H2
655.9
656.0
656.1
656.2
656.3
656.4
656.5
656.6
656.7
Wavelength /nm

Fig. 10

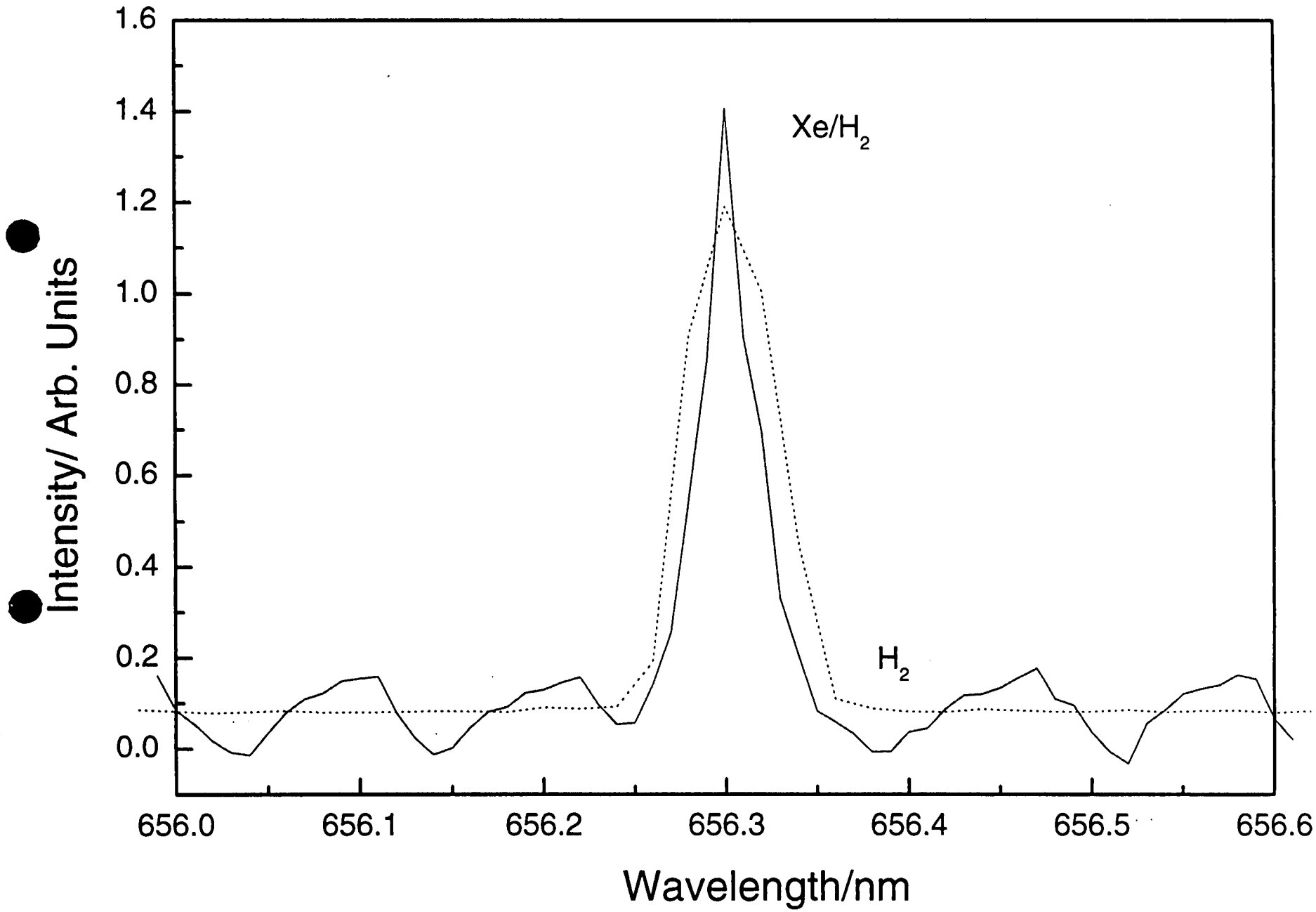
1.6
1.4
1.2
1.0
0.8
0.6
0.4
0.2
0.0
Intensity/ Arb. Units
Xe/H2
H2
656.0
656.1
656.2
656.3
656.4
656.5
656.6
Wavelength/nm

Fig. 11

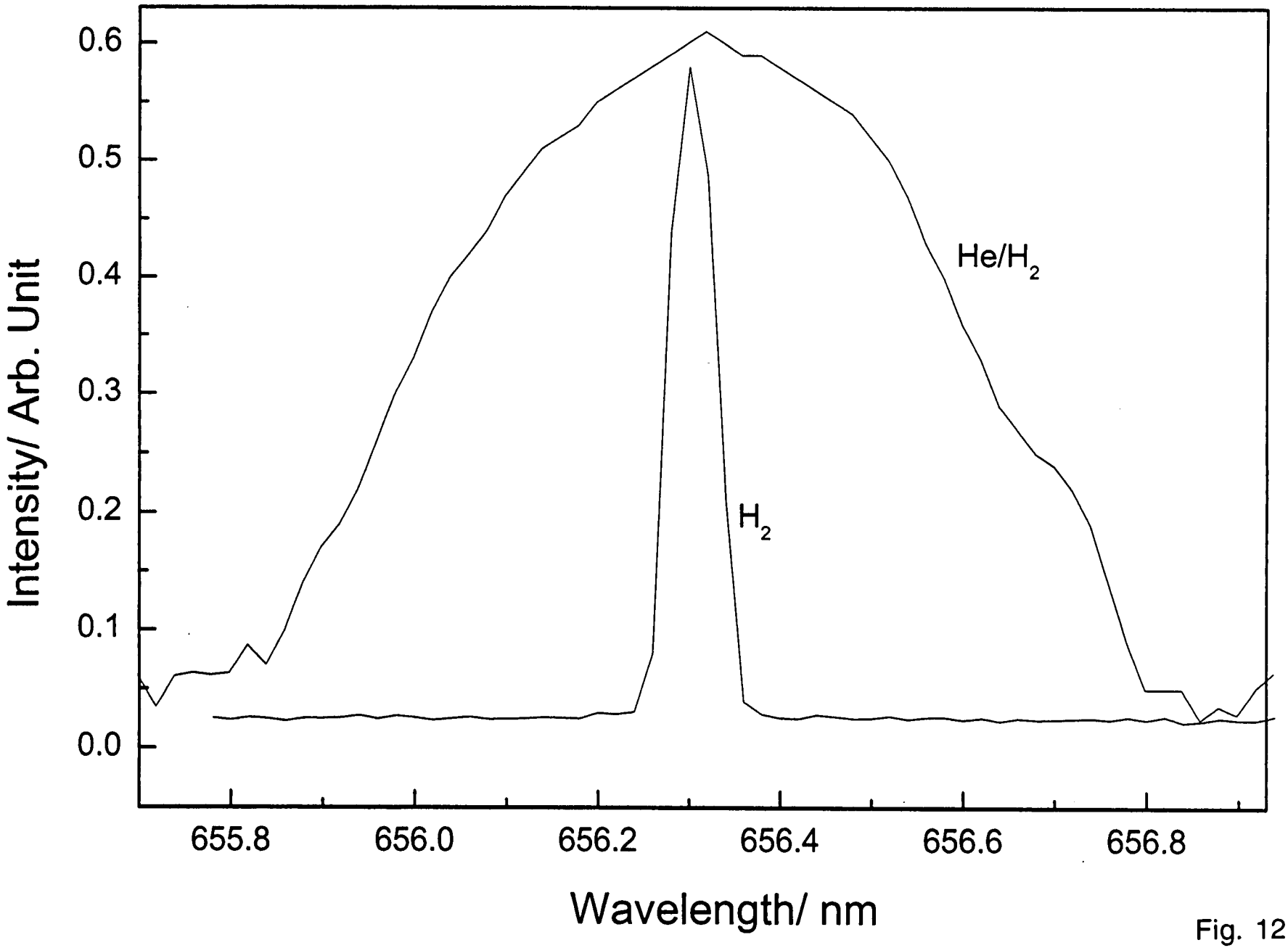
0.6
0.5
0.4
0.3
0.2
0.1
0.0
Intensity/ Arb. Unit
He/H2
H2
655.8
656.0
656.2
656.4
656.6
656.8
Wavelength/ nm

Fig. 12

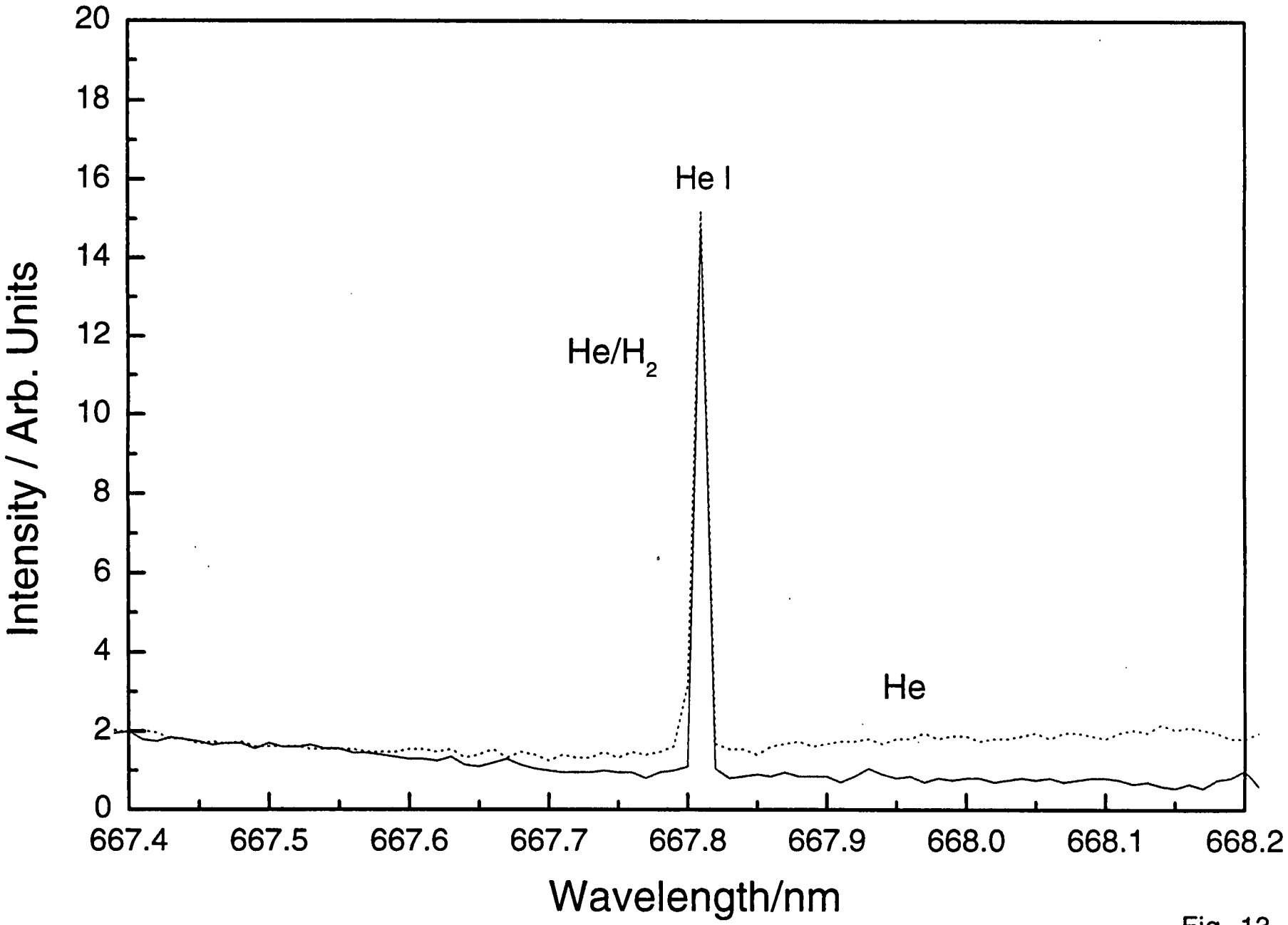
20
18
16
14
12
10
8
6
4
2
0
Intensity / Arb. Units
He I
He/H2
He
667.4
667.5
667.6
667.7
667.8
667.9
668.0
668.1
668.2
Wavelength/nm

Fig. 13

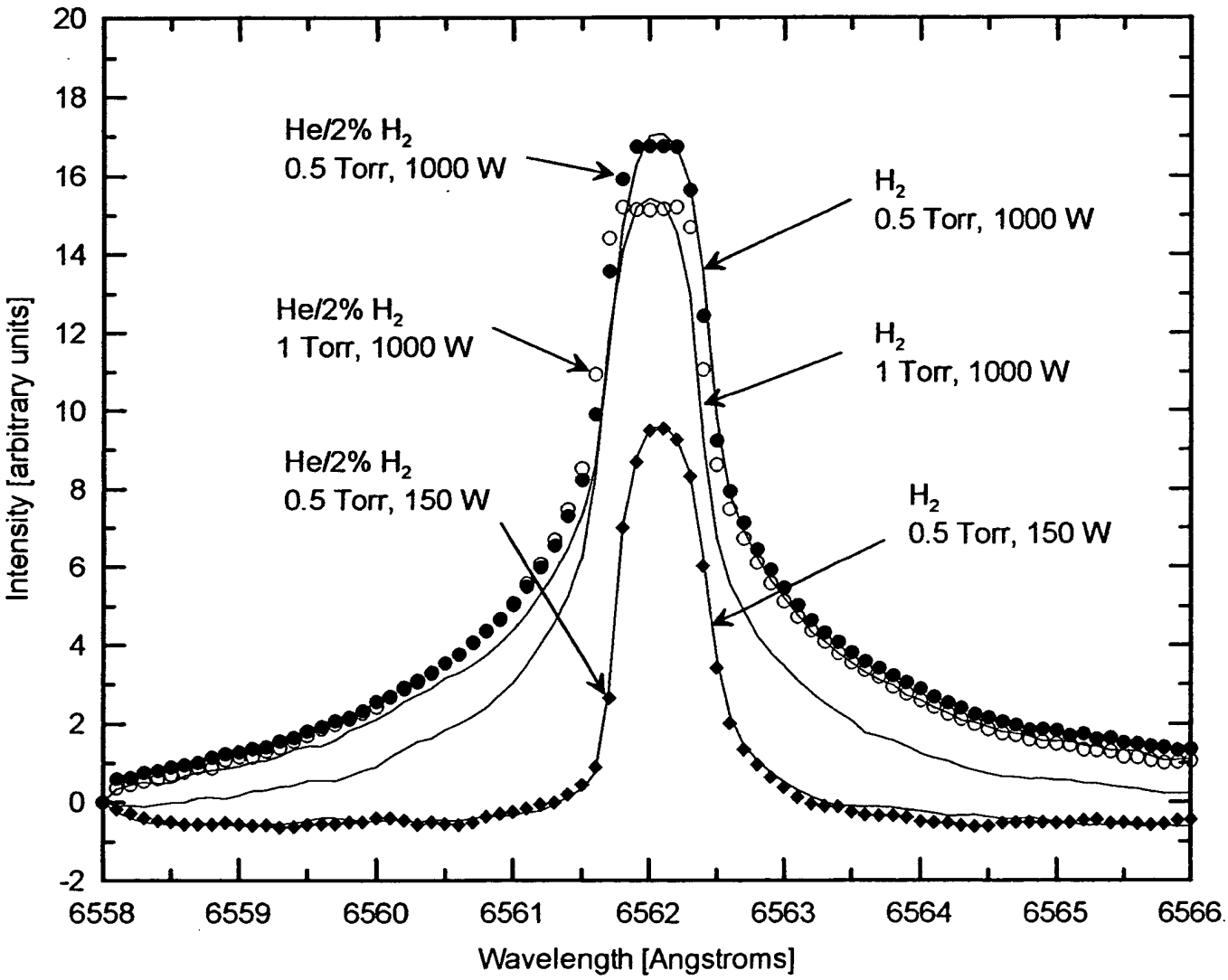
20
18
16
14
12
10
8
6
4
2
0
-2
Intensity [arbitrary units]
6558
6559
6560
6561
6562
6563
6564
6565
6566
Wavelength [Angstroms]
He/2% H2
0.5 Torr, 1000 W
H2
0.5 Torr, 1000 W
He/2% H2
1 Torr, 1000 W
H2
1 Torr, 1000 W
He/2% H2
0.5 Torr, 150 W
H2
0.5 Torr, 150 W

Fig. 14

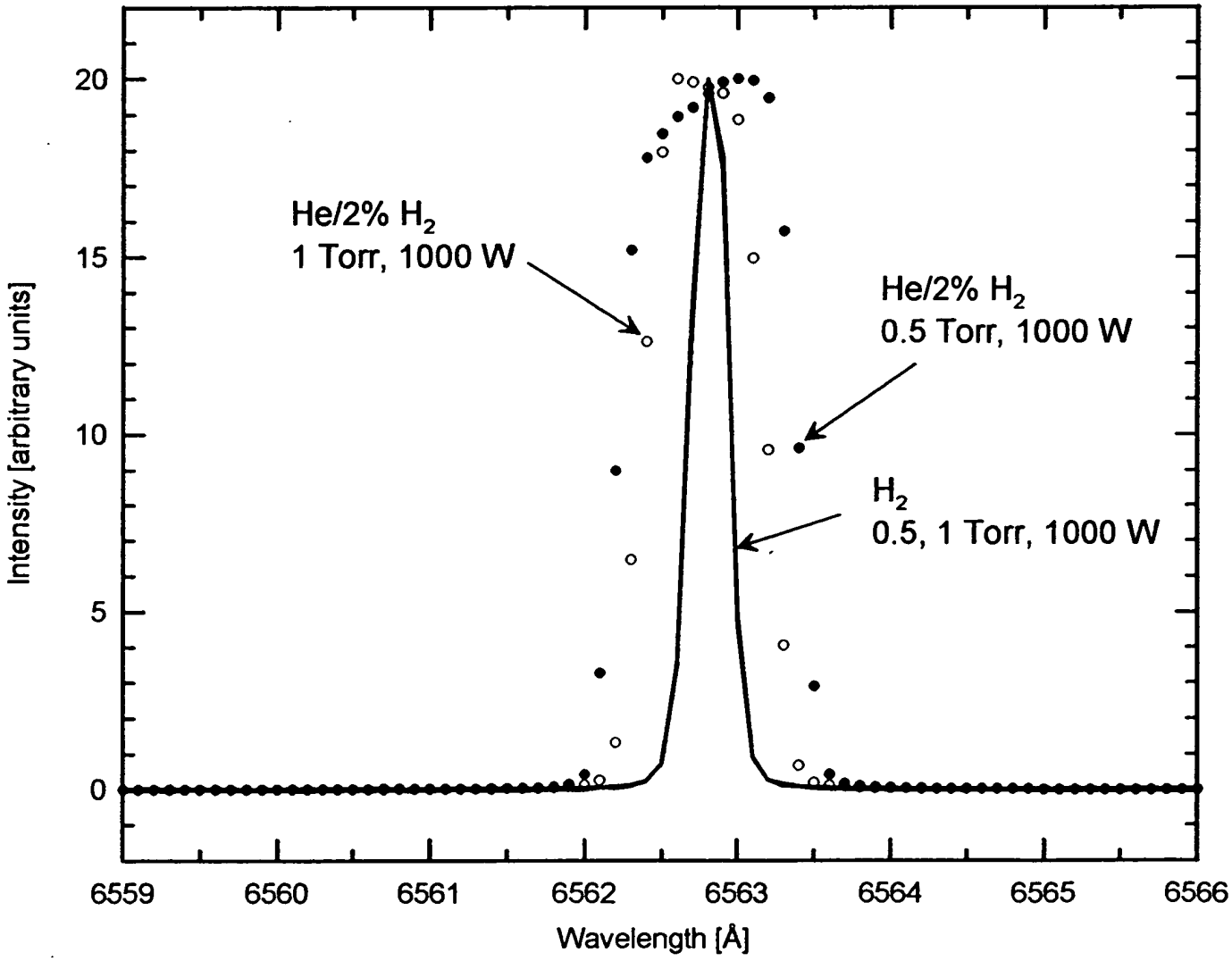
20
15
10
5
0
Intensity [arbitrary units]
He/2% H2
1 Torr, 1000 W
He/2% H2
0.5 Torr, 1000 W
H2
0.5, 1 Torr, 1000 W
6559
6560
6561
6562
6563
6564
6565
6566
Wavelength [Å]

Fig. 15

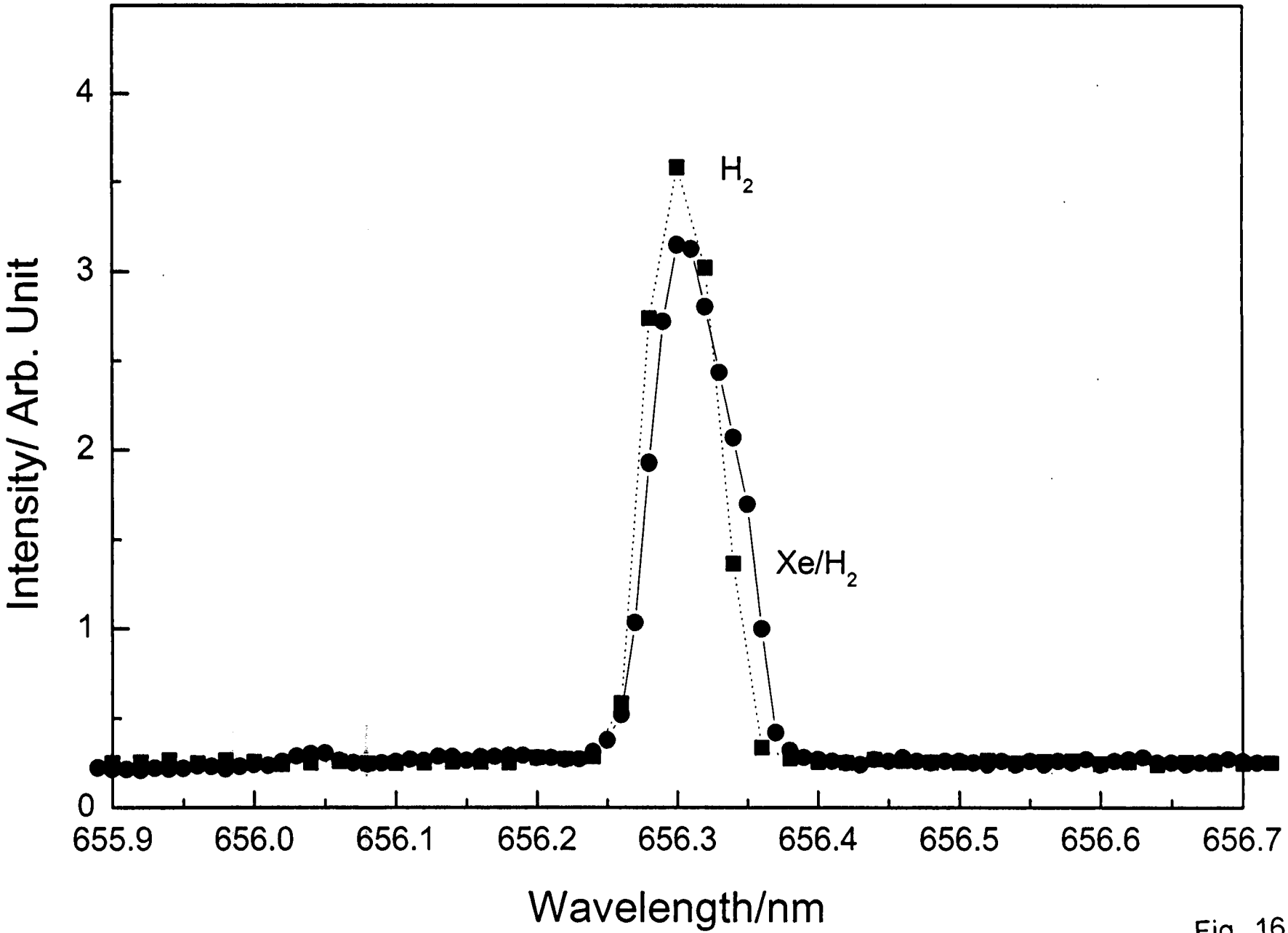
Intensity/ Arb. Unit
0
1
2
3
4
655.9
656.0
656.1
656.2
656.3
656.4
656.5
656.6
656.7
Wavelength/nm
H2
Xe/H2

Fig. 16

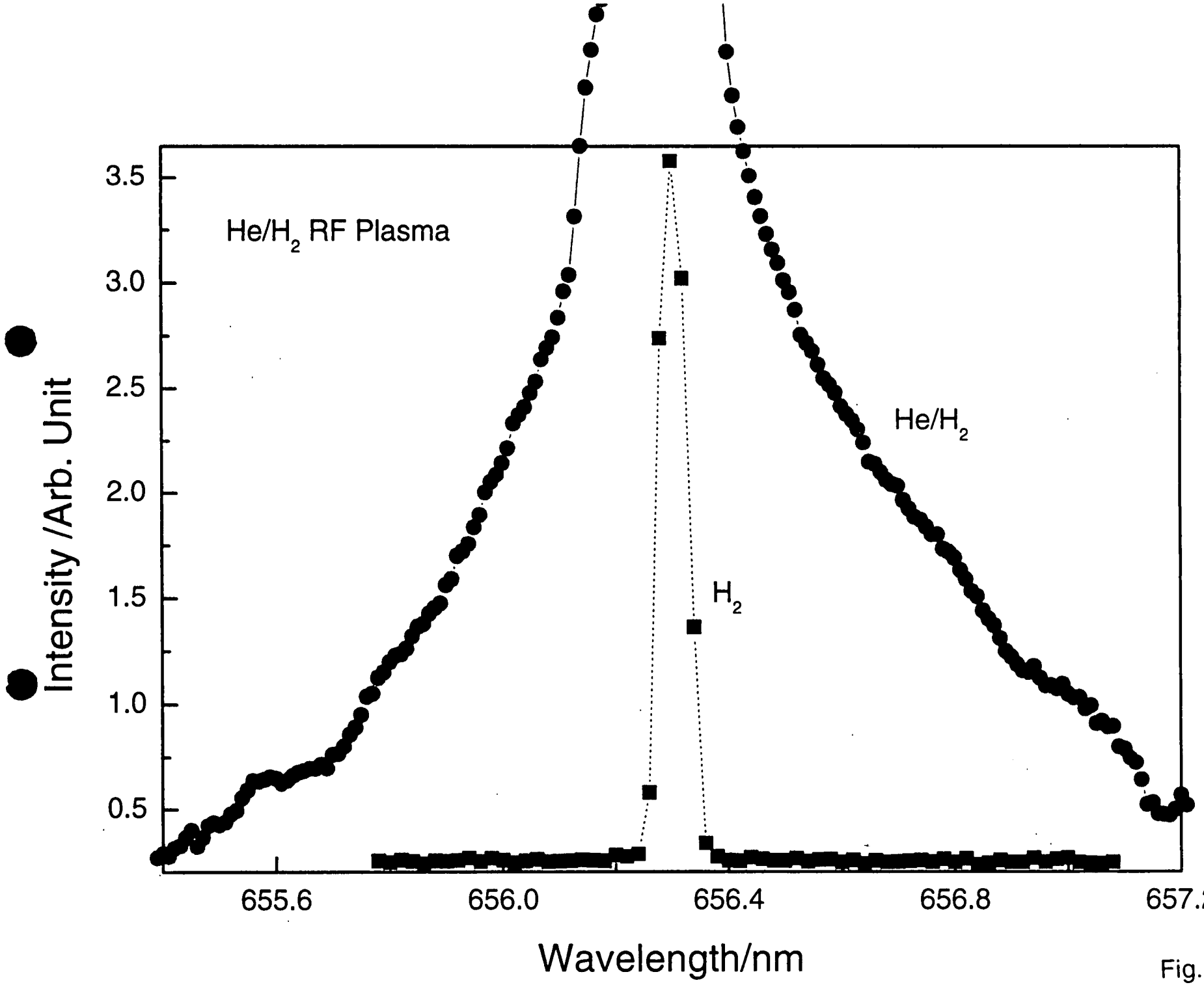
He/H2 RF Plasma
He/H2
H2
Intensity /Arb. Unit
Wavelength/nm
3.5
3.0
2.5
2.0
1.5
1.0
0.5
655.6
656.0
656.4
656.8
657.2

Fig. 17

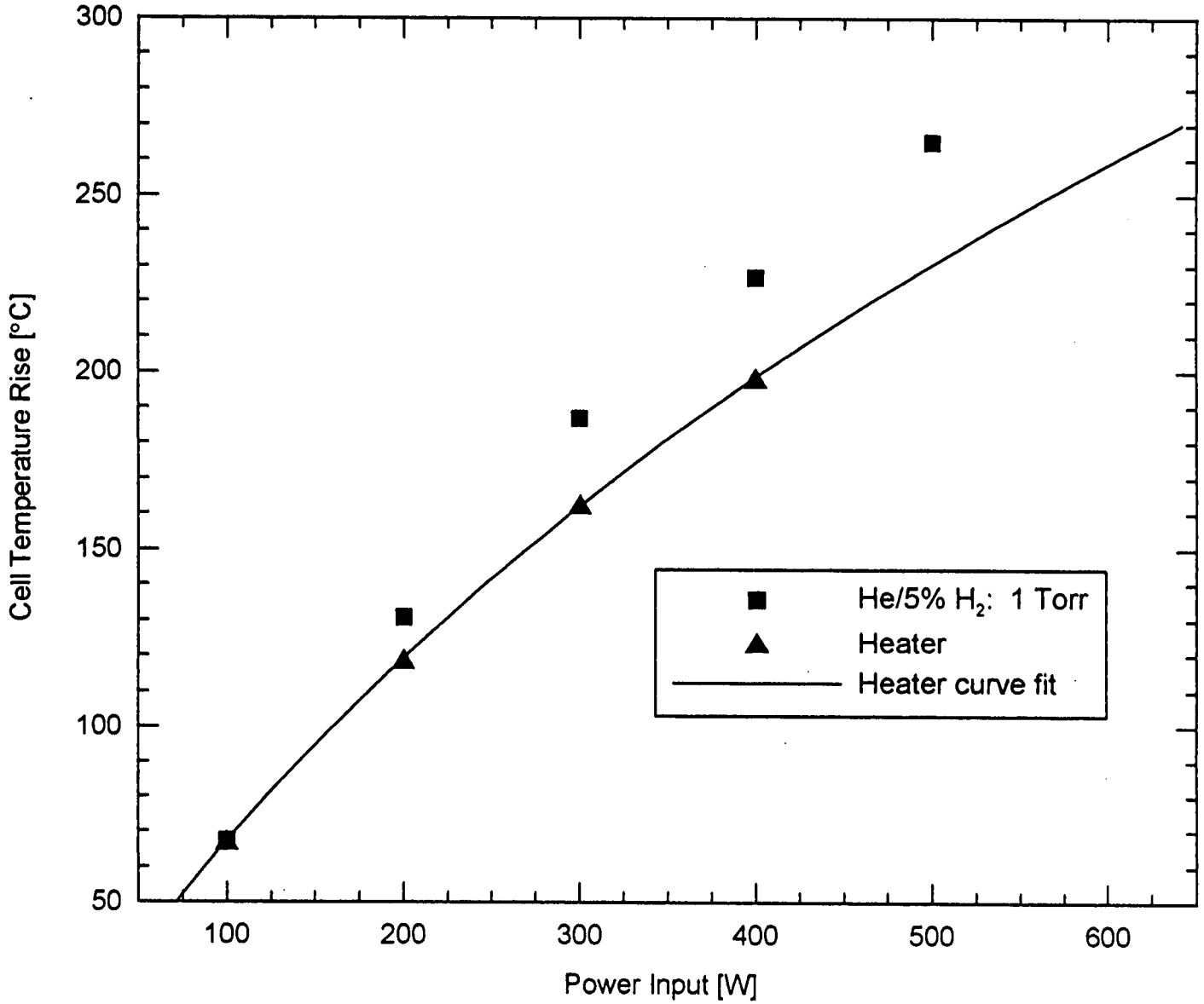
300
250
200
150
100
50
Cell Temperature Rise [°C]
100
200
300
400
500
600
Power Input [W]
He/5% H_2: 1 Torr
Heater
Heater curve fit

Fig. 18

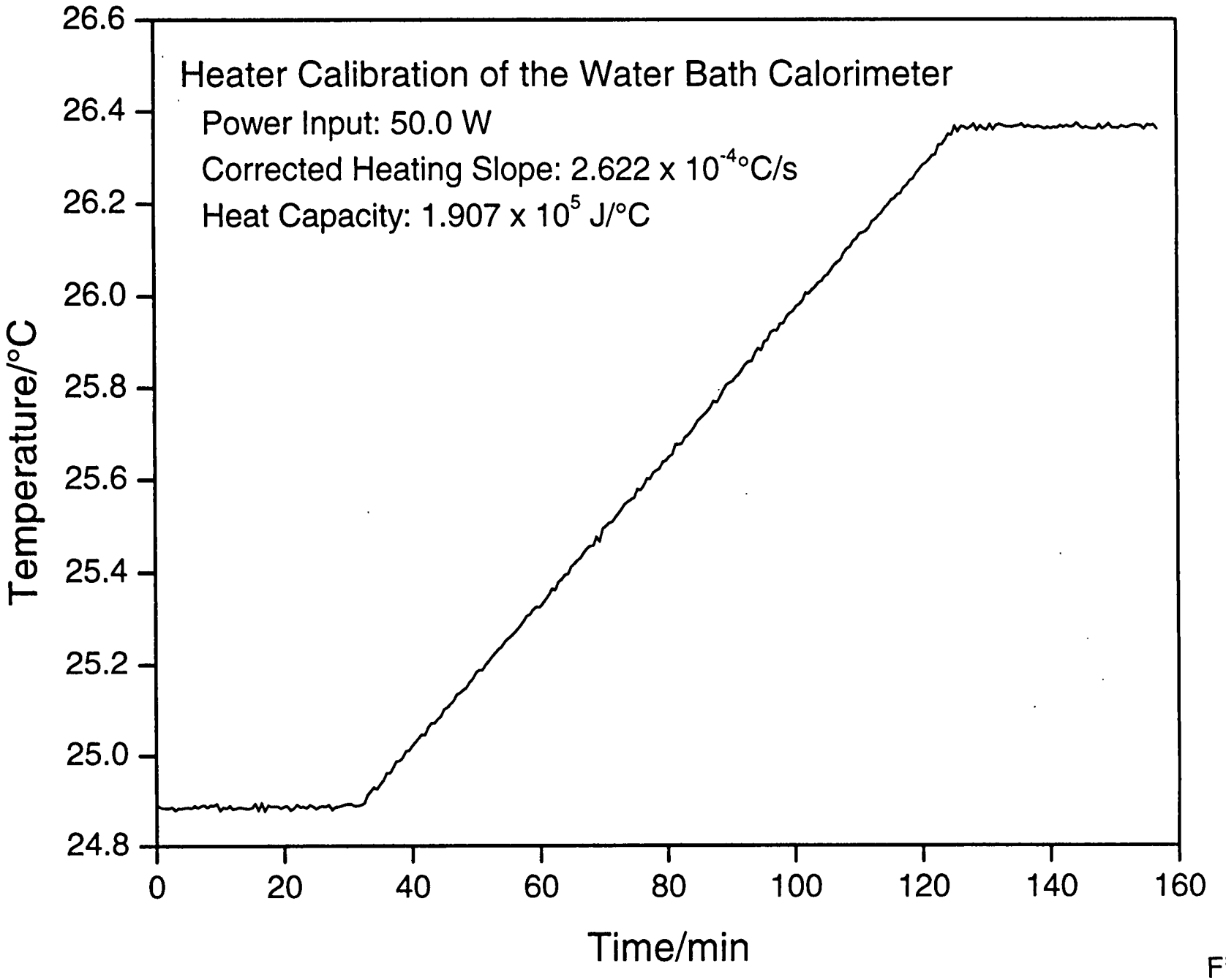
Heater Calibration of the Water Bath Calorimeter
Power Input: 50.0 W
Corrected Heating Slope: 2.622 x 10^-4 °C/s
Heat Capacity: 1.907 x 10^5 J/°C
Temperature/°C
26.6
26.4
26.2
26.0
25.8
25.6
25.4
25.2
25.0
24.8
0
20
40
60
80
100
120
140
160
Time/min

Fig. 19

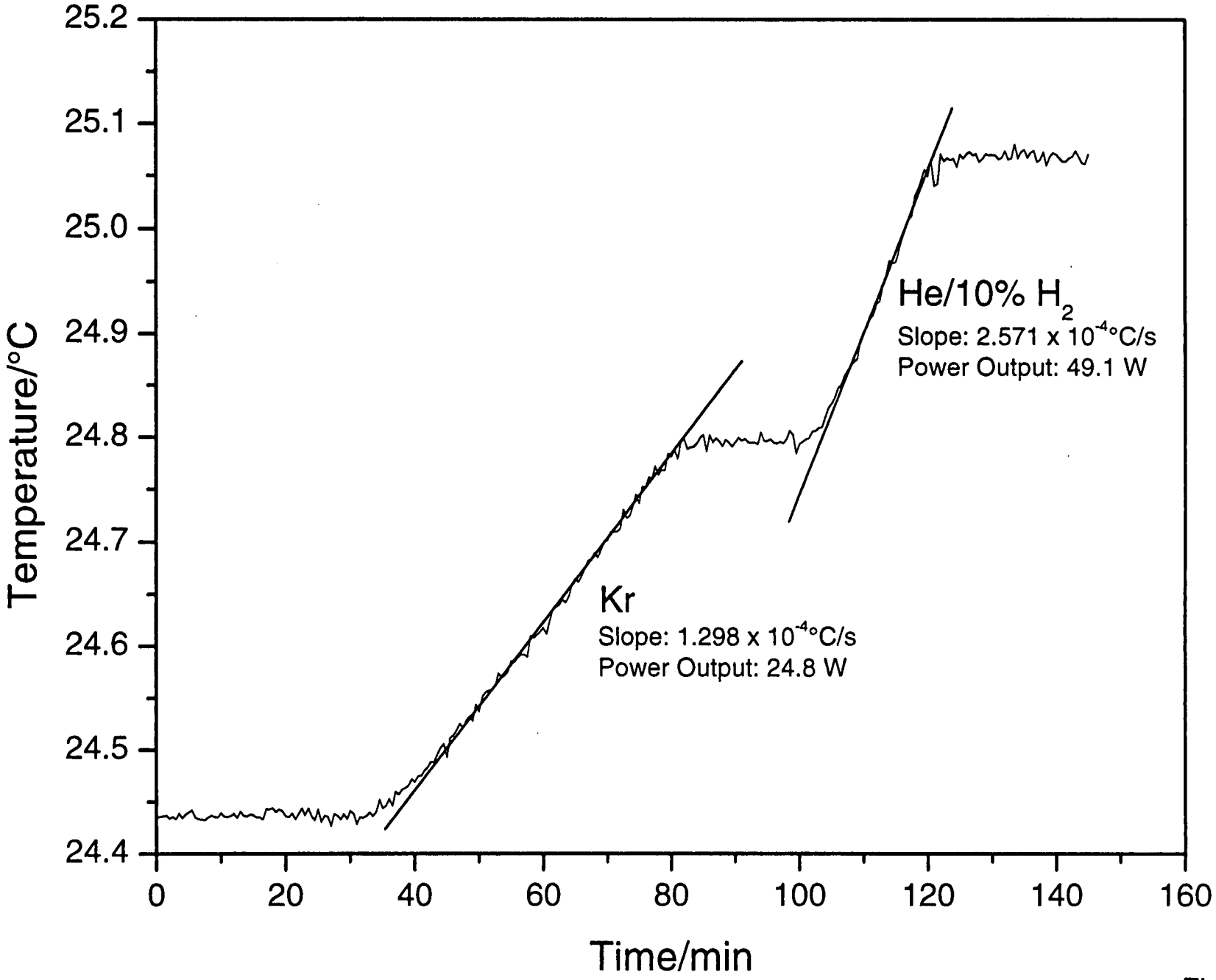
25.2
25.1
25.0
24.9
24.8
24.7
24.6
24.5
24.4
Temperature/°C
0
20
40
60
80
100
120
140
160
Time/min
He/10% H2
Slope: 2.571 x 10-4°C/s
Power Output: 49.1 W
Kr
Slope: 1.298 x 10-4°C/s
Power Output: 24.8 W

Fig. 20

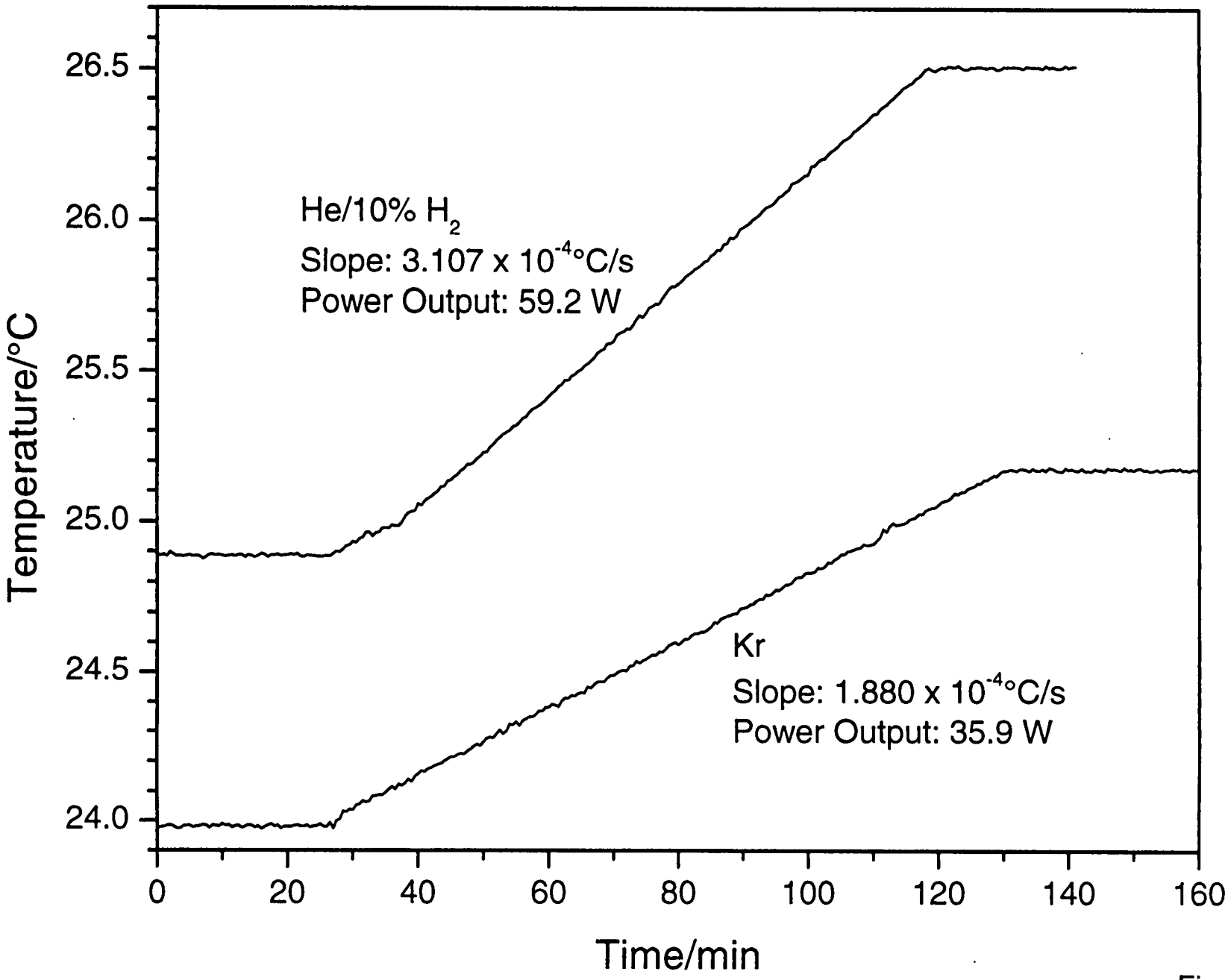
26.5
26.0
25.5
25.0
24.5
24.0
Temperature/°C
He/10% H2
Slope: 3.107 x 10-4°C/s
Power Output: 59.2 W
Kr
Slope: 1.880 x 10-4°C/s
Power Output: 35.9 W
0
20
40
60
80
100
120
140
160
Time/min

Fig. 21

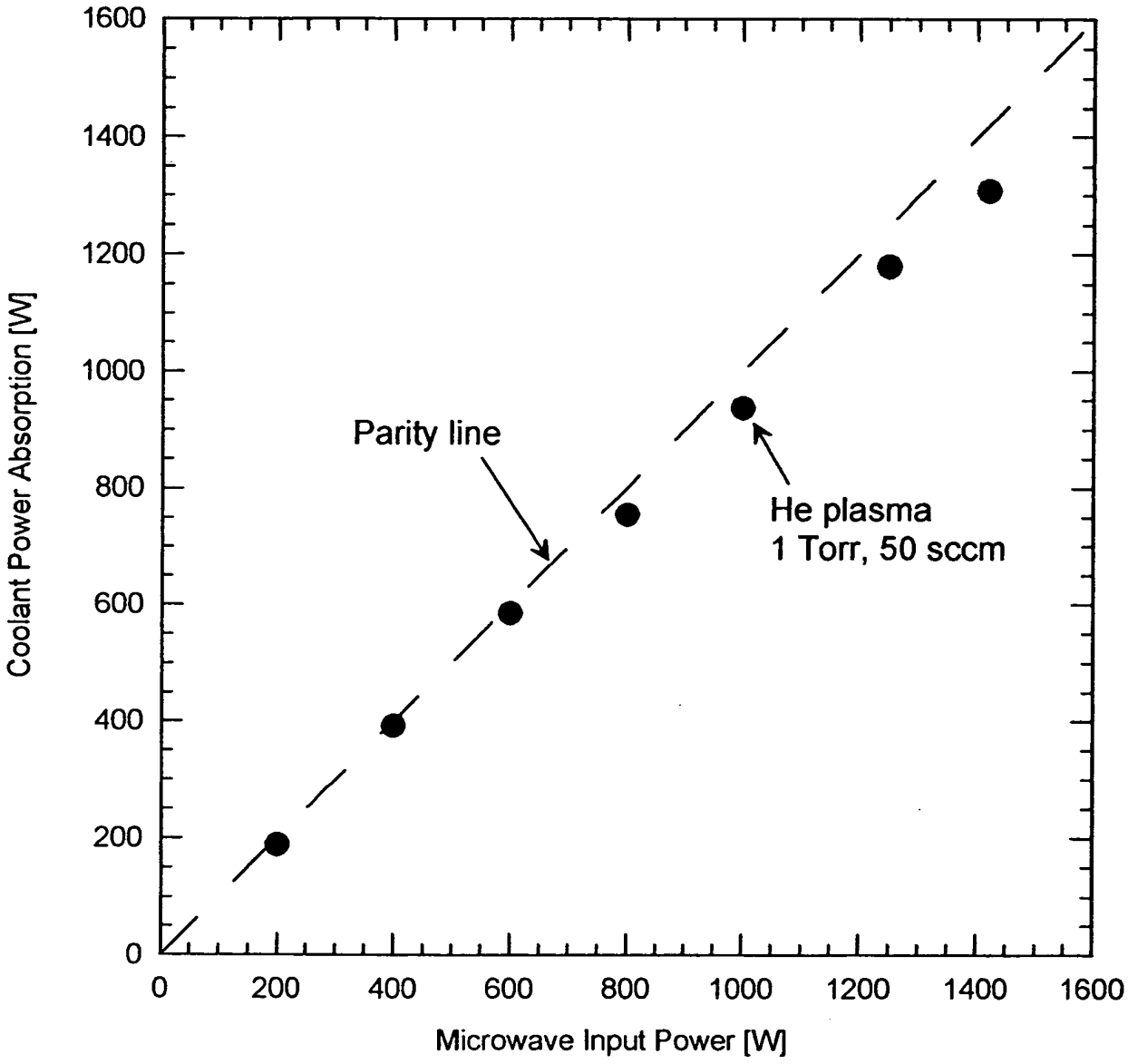
Coolant Power Absorption [W]
Microwave Input Power [W]
Parity line
He plasma
1 Torr, 50 sccm
0
200
400
600
800
1000
1200
1400
1600

Fig. 22

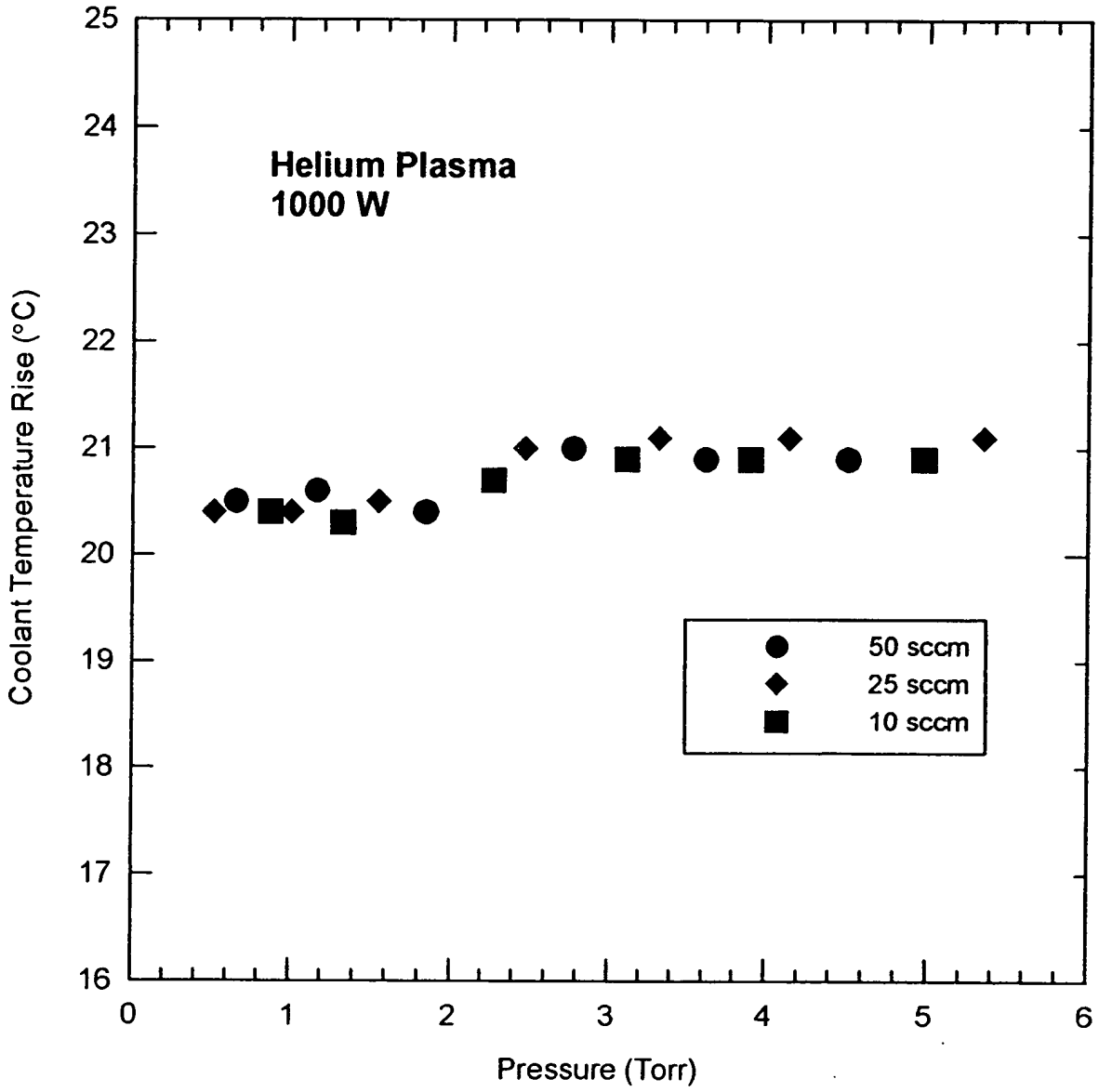
Helium Plasma
1000 W
Coolant Temperature Rise (°C)
Pressure (Torr)
50 sccm
25 sccm
10 sccm
25
24
23
22
21
20
19
18
17
16
0
1
2
3
4
5
6

Fig. 23

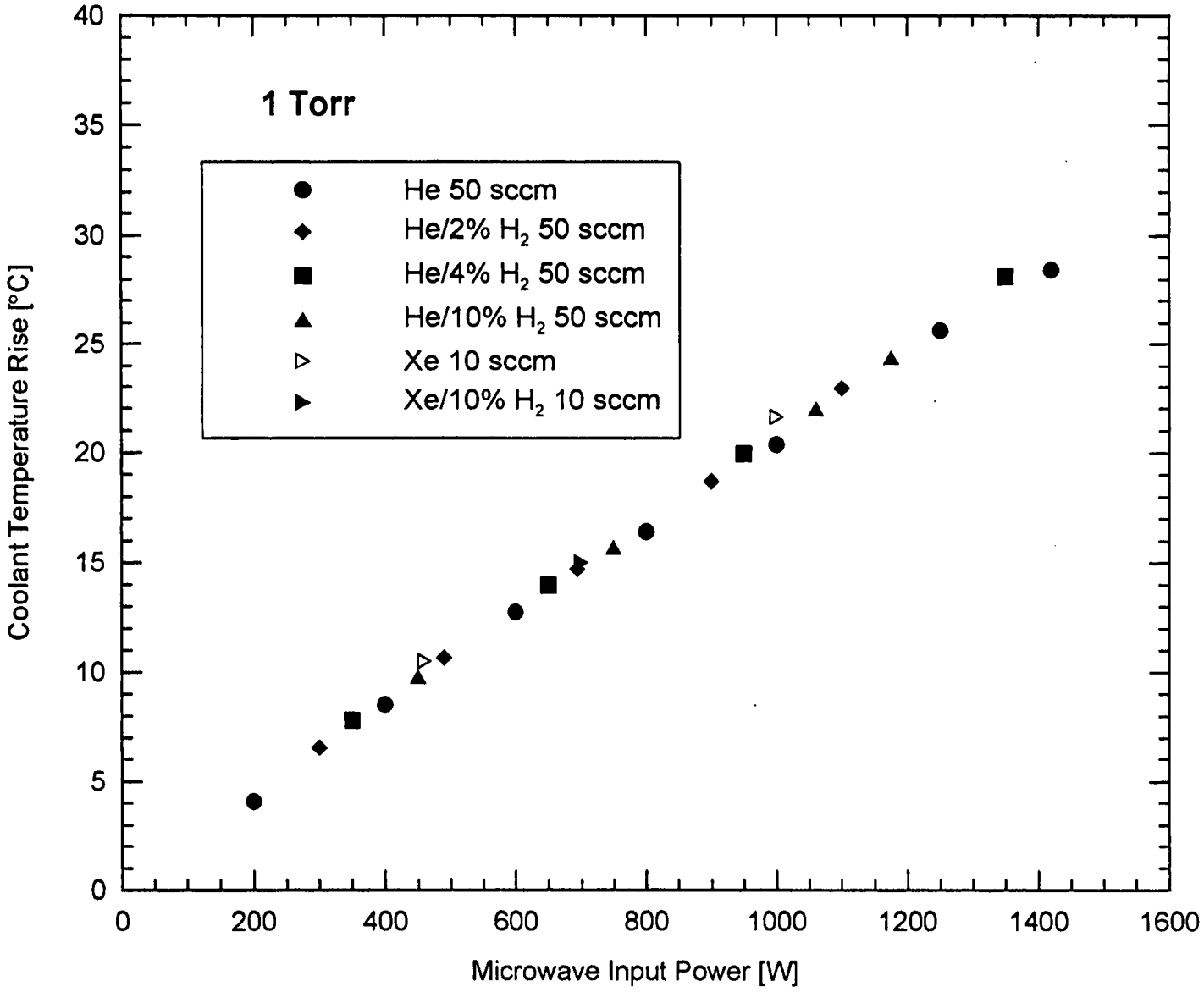
1 Torr
He 50 sccm
He/2% H2 50 sccm
He/4% H2 50 sccm
He/10% H2 50 sccm
Xe 10 sccm
Xe/10% H2 10 sccm
Coolant Temperature Rise [°C]
Microwave Input Power [W]
0
5
10
15
20
25
30
35
40
0
200
400
600
800
1000
1200
1400
1600

Fig. 24